Journal of Volcanology and Geothermal Research 424 (2022) 107513

Contents lists available at ScienceDirect

Journal of Volcanology and Geothermal Research

journal homepage: www.journals.elsevier.com/journal-of-volcanology-and-geothermal-research

Thermal springs and active fault network of the central Colca River basin, Western Cordillera, Peru

Andrzej Tyc [a], Krzysztof Gaidzik [a,*], Justyna Ciesielczuk [a], Pablo Masías [b], Andrzej Paulo [c], Adam Postawa [c], Jerzy Żaba [a]

[a] Institute of Earth Sciences, Faculty of Natural Sciences, University of Silesia, Będzińska 60, 41-200 Sosnowiec, Poland
[b] Observatorio Vulcanológico del INGEMMET (OVI), Barrio Magisterial 2 B-16 Yanahuara, Arequipa, Peru
[c] Faculty of Geology, Geophysics and Environmental Protection, AGH University of Science and Technology, Mickiewicza 30, 30-059 Kraków, Poland

ARTICLE INFO

Keywords:
Thermal springs
Hydrogeochemistry
Stable isotopes
Efflorescences
Active faults
Peru

ABSTRACT

Thermal waters and vapor discharges (hot springs, geysers, solfataras, and fumaroles) are common phenomena in volcanic regions at active plate boundaries, and the Central Andes are no exception. The Colca River basin in S Peru is a highly diversified and complex thermal region with unresolved questions on the origin of thermal fluids, reservoir temperature, and connections with tectonic and/or volcanic activity. To answer these, we used hydrogeochemical analysis of 35 water samples from springs and geysers, together with isotopic ($\delta^{18}O$ and δD) analysis, chemical and mineral studies of precipitates collected in the field around these outflows, and field observations. We aimed (1) to recognize the geochemistry of thermal waters and precipitates in the central part of the Colca River basin, (2) to identify fluid sources and their origin, (3) to estimate the temperature of a potential geothermal reservoir, and (4) to discuss the regional active tectonic and volcanic framework of this geothermal region and mutual relationships.

Our results corroborate a heterogeneous and complex geothermal system in the central part of the Colca River basin, with contrasting hydrogeochemical and physical properties, variable isotope composition, different reservoir temperatures, and associated precipitates around thermal springs. Processes controlling water chemistry are closely related to the Ampato-Sabancaya magmatic chamber's activity and tectonic structures that allow complex interactions of meteoric waters with magmatic fluids and gases. With a considerable gradient of pressure owing to local relief and deep incision in the Colca Canyon, these processes led to the differentiation of the thermal waters into three main groups. (1) Chloride-rich, mainly sodium chloride, thermal waters are of meteoric origin but mature within the geothermal reservoir possibly fed by magma degassing. These waters' chemical and isotopic composition results from water-rock interaction and mixing with magmatic waters within the reservoir. These waters discharge at the bottom of the Colca Canyon and Valley, presenting a broad hydrogeochemical spectrum and highly variable mineral phases precipitating at the outflows. The reservoir temperature estimated for these waters ranges from 180 to 200 °C. The group of hottest springs and geysers at the bottom of the Colca Canyon waters are fully equilibrated, with the reservoir temperature ~ 240 °C. (2) Sulfate-rich waters are shallow meteoric waters heated by ascending gases that form an independent group referring to the local water circulation, often controlled by tectonic barriers. (3) Bicarbonate-rich waters are the intermediate meteoric waters, divided into two hydrochemical groups: waters partially equilibrated with reservoir rocks and more similar to chloride-rich waters or additionally enriched with SO_4 and more similar to sulfate-rich waters.

Studied thermal springs show a clear spatial correlation with active and seismogenic crustal W- to NW-tracing normal and strike-slip faults. These act as barriers to infiltrating meteoric waters, provide pathways to hydrothermal solutions and gases assisting in meteoric water heating, and yield passages for pressured by lithostatic load and heated waters to ascend to the surface.

* Corresponding author at: Institute of Earth Sciences, University of Silesia, Będzińska 60, 41-200 Sosnowiec, Poland.
E-mail addresses: andrzej.tyc@us.edu.pl (A. Tyc), krzysztof.gaidzik@us.edu.pl (K. Gaidzik), justyna.ciesielczuk@us.edu.pl (J. Ciesielczuk), pmasias@ingemmet.gob.pe (P. Masías), postawa@agh.edu.pl (A. Postawa), jerzy.zaba@us.edu.pl (J. Żaba).

https://doi.org/10.1016/j.jvolgeores.2022.107513
Received 19 November 2021; Received in revised form 16 February 2022; Accepted 18 February 2022
Available online 22 February 2022

1. Introduction

Worldwide examples of the numerous and diverse forms of thermal waters and vapor discharges (hot springs, geysers, solfataras, and fumaroles), occurring primarily in volcanic regions at active plate boundaries, which differ in water composition, temperature, hydrogeochemical and physical properties, corroborate that these form complex hydrogeological systems (e.g., Waring, 1965; Steinmüller and Zavala, 1997; Steinmüller, 2001; Pérez-Flores et al., 2016; Roquer et al., 2017; Cruz, 2018; González-Guzmán et al., 2019). However, the detailed analysis of hydrogeochemical features of natural fluid discharges, together with isotope characteristics, composition of efflorescences, might provide insights in comprehending physico-chemical processes acting at depth, i.e., water-rock interaction, mixing of deep fluids with meteoric waters, recognition of deep-seated inputs (hydrothermal, metamorphic and magmatic), and leads to understanding volcanic-tectonic-hydrological interactions (e.g., Tassi et al., 2006; Pérez-Flores et al., 2016; Roquer et al., 2017; Townend et al., 2017; Cruz, 2018; González-Guzmán et al., 2019). Understanding the type of geothermal system and the fluid source is considered crucial to the success of any commercial development (Zarrouk and McLean, 2019).

Thermal waters are common phenomena along the Andes of southern Peru (e.g., Steinmüller and Zavala, 1997; Steinmüller and Nuñez, 1998; Steinmüller and Huamani, 1999; Steinmüller, 2001; Huamaní, 2000, 2001; Huamaní and Valenzuela, 2003; Cruz, 2018) and northern Chile (e.g., Cortecci et al., 2005; Pérez-Flores et al., 2016), connected with neotectonic movements, volcanic activity and high heat flow resulting from of the subduction of the oceanic Nazca Plate beneath the western border of the continental South American Plate. Although the history of exploring and exploiting hot springs in this region began almost a hundred years ago, the mountainous sector of Arequipa, e.g., the central part of the Colca River drainage basin, remained hardly accessible and thus, unknown in this regard for many years. Over the years, various hydrogeochemical properties of Peruvian thermal waters have been studied, mentioning from 72 thermal springs in entire Peru (Waring, 1965), through >100 (Steinmüller, 2001), to 589 in South Peru (Vargas, 2010).

The Colca River basin appears to be a highly diversified thermal region; however, it is up to date not sufficiently studied. Questions on the origin of thermal fluids, reservoir temperature, or connections with tectonic and/or volcanic activity have not been addressed. Only the eastern part of this area (i.e., springs in the Colca Valley), with popular among tourists La Calera and Yanque thermal swimming pools, has been a subject of hydrogeochemical analysis (e.g., Steinmüller and Zavala, 1997; Steinmüller, 2001) but no general geothermal model was proposed. The western part (i.e., springs and geysers in the Colca Canyon) has not yet been a subject of a detailed hydrogeochemical analysis.

Thus, the main goals of this study are (1) to recognize the geochemistry of thermal waters and precipitates in the central part of the Colca River basin, (2) to identify fluid sources and their origin, (3) to estimate the temperature of a potential geothermal reservoir and (4) to discuss the regional active tectonic and volcanic framework of this geothermal region. To answer these questions, we used hydrogeochemical analysis of 35 water samples from springs and geysers located in the central part of the Colca River drainage basin, isotopic analysis, and chemical and mineral studies of precipitates collected in the field around these outflows, and field observations. Finally, we provide a conceptual model of the geothermal system in the central part of the Colca River basin that incorporates and combines topography, hydrogeochemical, and isotope data with main tectonic and volcanic features.

2. Study area

2.1. Geological and tectonic setting

The study area is located in the Colca River basin between Sibayo town in the east and the Mamacocha River in the west, covering both the Colca Valley and the Colca Canyon. Due to the spectacular landscape of the deepest canyon in the world, it is one of the most important tourist regions in Peru (e.g., Gałaś et al., 2018). Geologically it forms a part of the Western Cordillera of the Central Andes, being the polyphase back-arc to intra-arc formed within the South American continental plate over the subducted Nazca oceanic plate (Fig. 1A). Colca Canyon is a natural cross-section revealing several structural complexes (Palacios, 1995; Paulo, 2009): 1) Proterozoic crystalline basement belonging to Arequipa and Paracas massifs (Mamani et al., 2010); 2) Jurassic and Cretaceous siliciclastic and carbonate formations of the epicontinental sea, intensely folded and intruded by granitoid plutons during Peruvian orogeny; 3) Late Cretaceous – Paleogene molasse formations of back-arc and intra-arc basins gently folded and locally overthrusted, and emplaced by shallow-level intrusions in Incaic phase; 4) Late Oligocene-Miocene volcanic Tacaza Group; 5) Pliocene-Recent Central Volcanic Zone of the Andes, Barroso Group; 6) Quaternary Andagua volcanics (Gałaś, 2014) and lacustrine-alluvial deposits in the Colca Valley (Kukulak et al., 2016; Fig. 1B). Lacustrine sediments and coarse-grained deltaic intercalations dominate the Colca Valley. Some tributary valleys carry thick Quaternary travertine deposits, which are karstified.

This area is tectonically intensively deformed, including folds and faults of various generations up to currently forming landslide structures posing a hazard to local communities (e.g., Żaba et al., 2012, 2013; Benavente et al., 2017; Gaidzik et al., 2020; Gaidzik and Więsek, 2021). Large subduction earthquakes and crustal events corroborate the recent seismic activity in this region on the overriding plate of magnitude, usually not exceeding 6.0 (e.g., Antayhua et al., 2001, 2002). Extensional discontinuities seem to carry more water than Mesozoic stratified layers of low porosity, intercalated by shales. Otherwise, Cenozoic formations, especially Quaternary travertines and fluvial gravel cones along paleolakes, and to a minor scale, some lava flows of Tacaza and Barroso groups are water-bearing. Their real permeabilities were not measured as yet. Wohletz and Heiken (1992) report typical permeabilities for all rock types ranging from 10^{-20} m^2 (0.01 μDarcy) to 10^{-7} m^2.

This central part of the study area is also characterized by the volcanic activity related to Sabancaya, which is the youngest and the most active of the three volcanoes of the Ampato-Sabancaya Volcanic Complex (ASVC), which also includes Hualca Hualca to the north (Fig. 1A; Boixart et al., 2020; Reath et al., 2020). These volcanoes are mostly composed of andesitic and dacitic lava flows and pyroclastic deposits (Rivera et al., 2015; Samaniego et al., 2016), being surrounded by an extensive system of active faults and lineaments related to high seismicity (e.g., Żaba et al., 2013; Jay et al., 2015; Reath et al., 2020; Gaidzik and Więsek, 2021). Ampato is a dormant stratovolcano with no historical activity, composed of three volcanic cones overlying an older eroded volcanic edifice (Samaniego et al., 2016). The Pleistocene Hualca Hualca volcano is believed to be extinct.

Hydrothermal activity is observed near Pinchollo on the Hualca Hualca slope, but it could be of tectonic origin related to W-trending faults (Ciesielczuk et al., 2013). Strong pre-eruptive seismicity at Sabancaya seems to be a consequence of magmatic intrusions destabilizing tectonic faults critically stressed by regionally high fluid pressures. High fluid pressure observed at Sabancaya will likely promote fault creep driven by static stress transfer from the inflation source. It is considered that the combination of high pore fluid pressures with sufficiently large offset magmatic inflation can promote strong earthquakes during volcanic unrest (MacQueen et al., 2020).

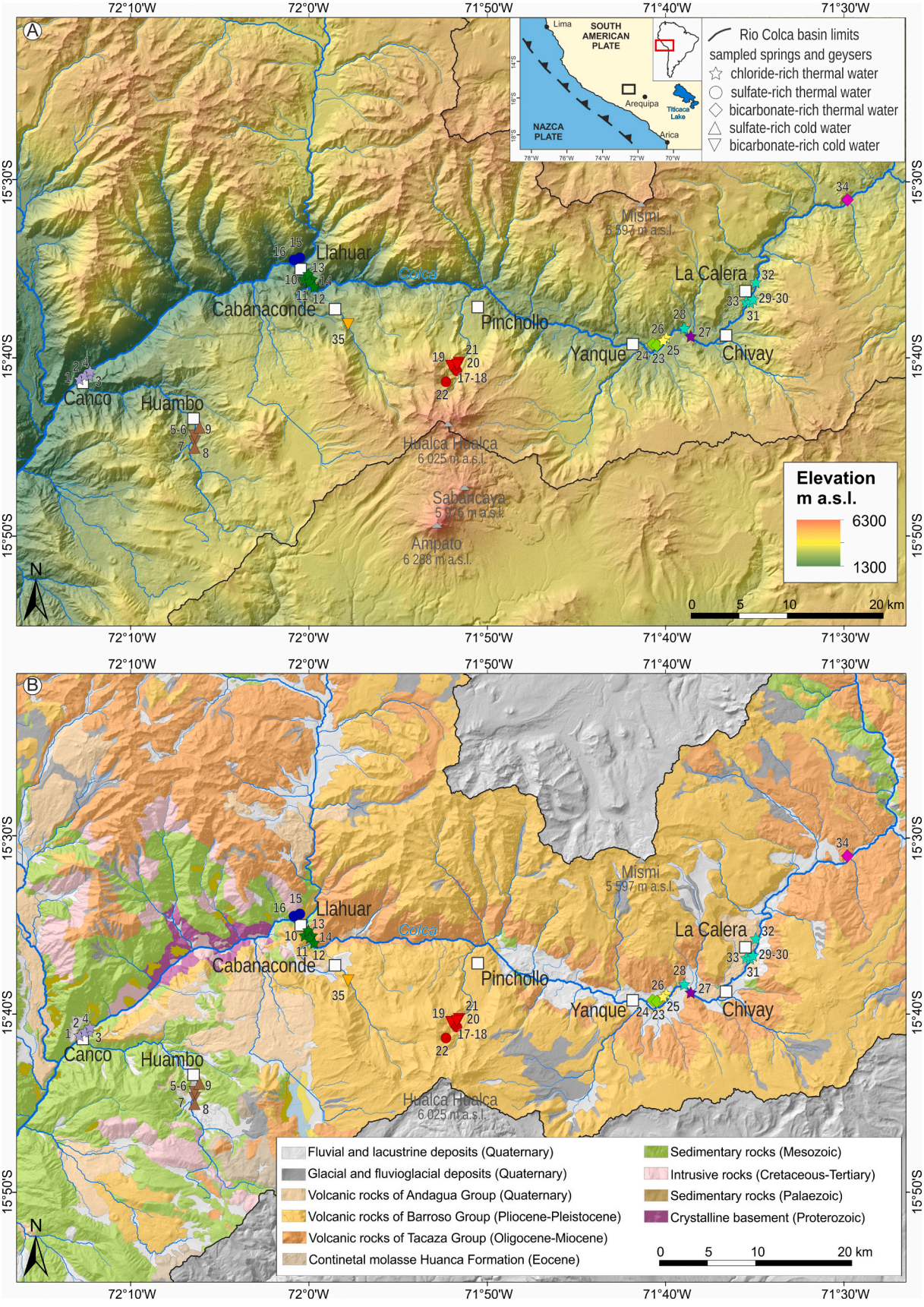

Fig. 1. Location of the studied thermal springs (no. 1–35) in the central Colca River basin. A – Shaded relief map (30 m resolution digital elevation model, DEM from Shuttle Radar Topography Mission, SRTM (Farr and Kobrick, 2000f; https://earthexplorer.usgs.gov); B – Lithology, symbols as in Fig. 1A.

2.2. Climate setting

The climate of the Colca River basin is considered temperate and dry, with seasonal rains from December to March–April (Zavala et al., 2014), and significant variations in temperature and precipitation depending on the elevation a.s.l. In the highest areas, i.e.,> 4500 m a.s.l., the mean annual temperature ranges from 1 to 6 °C, and mean annual precipitation exceeds 620 mm. In medium altitudes (4000–2800 m a.s.l.), the mean annual temperature varies from 6.5 to 17.6 °C, and recorded annual precipitation ranges 150–600 mm. In the lowest zones of the western part of the study area, the temperature does not vary considerably, maintaining an annual mean of 19 °C. In these regions, the

Fig. 2. Chosen thermal springs and geysers (sampling sites) in the central Colca River basin: A – zone of thermal springs in Canco (No. 3, 4); B – geyser in Paclla (No. 13); C – Pinchollo geyser (No. 17–18); D – Puye thermal spring (No. 26); E – Sallihua thermal spring (No. 28); F – La Calera thermal spring (No. 29, 30); G – thermal spring above La Calera (No. 32); H – thermal spring below la Calera (No. 33).

precipitation is very limited, usually not exceeding an annual amount of 150 mm (Zavala et al., 2014).

3. Sampling and methods

The studied thermal springs, geysers, and solfataras are located in eight clusters distributed in two different sectors of the central Colca River basin – Colca Valley and Canyon. Five belong to the Chivay geothermal group (according to Steinmüller and Zavala, 1997; Steinmüller, 2001; Vargas and Cruz, 2010) situated along the Colca River Valley upstream of Yanque (No. 23–34 on Figs. 1 & 2, Tables 1 & 2). The next three– Canco, Paclla, and Llahuar – are at the bottom of the Colca Canyon (No. 1–3, 10–14, and 15–16, respectively, Figs. 1 & 2, Tables 1 & 2). Additionally, our studies covered geothermal sites on the northern slope of extinct Hualca Hualca volcano, south of Pinchollo (No. 17–22), and cold springs in the areas of Huambo (No. 5–9) and Cabanaconde (No. 35), all located in the southern segment of the Colca River basin (Fig. 1, Tables 1 and 2).

Sampling of springs and geysers was carried out during two field campaigns of the Polish Scientific Expedition to Peru: in September 2012 and August–September 2017. Thus, water samples were collected during the dry season to avoid mixing with meteoric waters. Physical parameters are compiled in Table 1. Thirty-five sets of water samples were collected (16 and 19, respectively) using polyethylene bottles of high density. They were analyzed in the Water Analysis Laboratory at the University of Silesia in Katowice (Poland). Water temperatures, pH, and electrical conductivity were measured in the field using portable pH meter CP-315 and conductivity meter CC-315, both with temperature sensors, with an accuracy of ±0.1 °C, ±0.01 pH, and ± 0.1% (up to 19.999 mS/cm) or ± 0.25% (above 20.00 mS/cm), respectively. Discharge of springs was estimated if possible.

Water samples for analysis of cations and dissolved metals (Ca^{2+}, Mg^{2+}, Na^{+}, K^{+}, NH_4^{+}, Li^{+}) were filtered through a 0.45 μm membrane filter and acidified using ultra-pure HNO_3^{-}. Non-preserved samples were used to determine anions (F^{-}, Cl^{-}, NO_2^{-}, NO_3^{-}, Br^{-}, PO_4^{3-}, SO_4^{2-}) and for the isotopic analysis of oxygen and hydrogen. Both cations and anions were analyzed by ion chromatography using Methron 850 Professional Ion Chromatograph with separate Metrosept C4–150 and A-supp 7–250 columns for cations and anions, respectively. Quantification limit and precision are 0.01 mg/L for Ca^{2+}, Mg^{2+}, NO_3^{-} and SO_4^{2-}, 0.02 mg/L for Na^{+}, NH_4^{+}, Li^{+}, F^{-}, Cl^{-}, NO_2^{-}, Br^{-} and PO_4^{3-} or 0.03 mg/L in case of K^{+}. Alkalinity was measured volumetrically by titration using 0.05 N HCl and methyl-orange as a colorimetric indicator. The cation-anion balance in meq/L is less than ±5%, except for two hot water samples taken in Llahuar (No. 15 and 16), where the balance error was +10–11%.

Additionally, in this paper, we discuss the results of the thermal springs analyses carried out by the Instituto Geológico Minero y Metalúrgico (INGEMMET) of Peru in the framework of the hydrogeochemical monitoring (Table S1). Similar to our sampling methods, basic physicochemical properties of spring waters were determined in the field, alkalinity was determined by titration. Water analyses were performed at the INGEMMET Chemical Laboratory in Lima with the use of ion chromatography (Dionex ICS 5000) for the determination of anions (F^{-}, Cl^{-}, NO_2^{-}, NO_3^{-}, SO_4^{2-}) and inductively coupled plasma optical emission spectrometry (ICP-OES) – VARIAN for cations (incl.

Table 1
Physicochemical characteristics of water samples.

No.	Location. discharge type	Date	Coordinates		Altitude [m a.s.l.]	T_w *	EC*	pH*	Q**
			Latitude	Longitude					
1	Canco, springs	11.09.2012	15°41′07.3″	72°12′47.1″	1393	51	5.0–5.2	7.59	n.d.
2		11.09.2012	15°41′07.3″	72°12′47.1″	1393	62	5.2–5.3	7.17	n.d.
3		28.08.2017	15°41′03.7″	72°12′44.3″	1400	66.4	6.0	n.d.	0.2
4		28.08.2017	15°41′01.8″	72°12′43.3″	1382	72.7	5.7	n.d.	1
5	Huambo, springs	13.09.2012	15°44′25.4″	72°06′27.1″	3362	17–17.3	1.1	6.80	~100
6		1.09.2017	15°44′25.1″	72°06′24.4″	3351	17.1	1.5	7.02	>100
7		14.09.2012	15°44′25.4″	72°06′27.1″	3362	17–17.2	1.1	6.74	~50
8		1.09.2017	15°44′28.1″	72°06′27.0″	3347	16.1	1.5	7.15	5–10
9		1.09.2017	15°44′23.1″	72°06′26.9″	3347	16.9	1.6	7.17	1–2
10	Paclla, geyser	3.09.2017	15°35′44.2″	71°59′58.6″	2130	93.5	4.6	8.93	4.60
11	Paclla, spring	3.09.2017	15°35′44.0″	71°59′58.9″	2132	89	4.2–4.3	8.34	4.2–4.31
12		3.09.2017	15°35′42.2″	71°59′56.9″	2128	91	3.5	n.d.	3.54
13	Paclla, geyser	3.09.2017	15°35′43.7″	71°59′58.7″	2134	93	4.5	n.d.	4.46
14	Paclla, spring	3.09.2017	15°35′43.2″	71°59′58.8″	2131	50.8	4.3	8.61	4.27
15	Llahuar, springs	5.09.2017	15°34′52.0″	72°00′37.0″	2098	32.6	2.4	8.19	<5
16		5.09.2017	15°34′52.3″	72°00′36.6″	2098	38.1	2.7	8.15	<5
17	Pinchollo, geyser	16.09.2012	15°40′30.0″	71°51′42.9″	4382	~80	0.3	8.06	~10
18		5.09.2017	15°40′30.0″	71°51′42.7″	4337	86	0.6	8.37	n.d.
19	Pinchollo, springs	16.09.2012	15°40′30.0″	71°51′42.9″	4385	30–40	1.2	6.66	0.1
20		16.09.2012	15°40′30.0″	71°51′42.9″	4393	~30	0.7	8.22	0.2
21		16.09.2012	15°40′30.0″	71°51′42.9″	4395	17–18	0.6	8.27	0.5
22	Hualca Hualca, solfatara	16.09.2012	15°41′04.2″	71°52′11.6″	4752	40–50	n.d.	n.d.	0.2
23	Yanque, springs	18.09.2012	15°39′18.6″	71°40′14.7″	3354	41	1.2	7.44	1.5
24		7.09.2017	15°39′16.7″	71°40′11.2″	3337	43.1	1.1	7.55	n.d.
25		7.09.2017	15°39′14.8″	71°40′7.9″	3329	59	3.6	6.68	n.d.
26	Puye, spring	7.09.2017	15°39′11.4″	71°40′06.7″	3324	71.3	4.2	6.91	5–10
27	Umaru, spring	7.09.2017	15°38′51.9″	71°38′38.0″	3438	70.2	6.9	6.30	n.d.
28	Sallihua, spring	18.09.2012	15°38′24.9″	71°38′51.9″	3386	47	1.7	7.00	4
29	La Calera, spring	17.09.2012	15°36′53.6″	71°35′12.7″	3636	68.9	5.5	6.76	2
30		9.09.2017	15°36′53.5″	71°35′12.8″		68.3	7.0	6.69	10
31	La Calera, spring below	17.09.2012	15°36′55.6″	71°35′23.9″	3614	49.1	3.5	6.73	1
32	La Calera, spring above	21.09.2012	15°35′46.9″	71°34′59.7″	3639	65.9	5.6	6.64	n.d.
33	La Calera, spring below	21.09.2012	15°36′53.8″	71°35′19.9″	3614	53	4.1	6.42	n.d.
34	Sibayo, spring	19.09.2012	15°31′07.2″	71°29′48.5″	3809	48.2	3.3	6.92	0.8
35	Cabanaconde, spring	3.09.2017	15°37′57.4″	71°57′48.1″	3450	18.6	0.4	8.62	20

T_w – water temperature in °C, EC – electrical conductivity in μS/cm, Q - spring or geyser discharge in L/s, n.d. – not determined.
* Measured in the field.
** Measured or estimated in the field.

Table 2
Chemical and isotopic composition of water samples.

No.	Location. discharge type	T_w	EC*	pH*	Ca^{2+}	Mg^{2+}	Na^{+}	K^{+}	Li^{+}	HCO_3^{-}	F^{-}	Cl^{-}	NO_2^{-}	Br^{-}	NO_3^{-}	SO_4^{2-}	TDS	$\delta^{18}O$	δD	Hydrochemical types of water
1	Canco, springs	51.0	5015	7.59	223	43.1	924	52.8	n.d.	641	0.00	952	0.00	1.67	1.94	769	3609	n.d.	n.d.	Na-Cl-SO_4
2		62.0	5200	7.17	255	41.7	937	53.3	n.d.	784	1.54	955	0.00	1.53	2.7	779	3811	n.d.	n.d.	Na-Ca-Cl-SO_4-HCO_3
3		66.4	6030	7.68	152	15.1	1148	61.3	1.19	540	3.9	1337	n.d.	3.3	11.6	925	4197	−13.45	−103.7	Na-Cl-SO_4
4		72.7	5700	8.23	112	18.0	1081	58.0	1.11	420	3.5	1254	n.d.	3.1	11.3	905	3866	−13.5	−104.3	Na-Cl-SO_4
5	Huambo, springs	17.0	1121	6.80	243	32.6	40.6	5.7	n.d.	613	0.41	36.3	0.00	0.00	1.33	314	1287	n.d.	n.d.	Ca-HCO_3-SO_4
6		17.1	1329	7.02	201	29.2	35.0	2.6	0.00	478	0.65	40.6	0.30	0.16	2.8	312	1103	−14.81	−106.8	Ca-HCO_3-SO_4
7		17.0	1128	6.74	245	32.2	39.7	5.0	n.d.	574	0.50	37.9	n.d.	n.d.	1.21	315	1250	n.d.	n.d.	Ca-HCO_3-SO_4
8		16.1	1352	7.15	212	29.6	34. 5	2.7	0.00	386	0.65	41.9	0.28	0.17	2.7	350	1060	−14.83	−108.3	Ca-SO_4-HCO_3
9		16.9	1433	7.17	214	30.0	49.9	3.0	0.00	283	0.70	68.0	0.28	0.19	2.6	381	1033	−14.58	−106.7	Ca-SO_4-HCO_3
10	Paclla, geyser	93.5	3590	8.93	24.7	0.00	595	60.2	1.71	73.2	5.4	897	n.d.	1.83	n.d.	335	1992	−12.54	−101.3	Na-Cl-SO_4
11	Paclla, springs	89.0	3450	8.34	43.2	0.00	618	63.2	1.67	88.5	5.0	896	n.d.	1.83	11.4	331	2058	−12.45	−101.8	Na-Cl-SO_4
12		91.0	3200	7.98	40.3	0.00	531	57.6	1.10	131	5.1	780	n.d.	1.64	11.3	291	1849	−13.13	−104.5	Na-Cl
13	Paclla, geyser	93.0	3510	8.24	29.3	0.00	621	69.7	1.87	74.4	5.7	920	n.d.	1.86	n.d.	346	2067	−12.44	−103	Na-Cl-SO_4
14	Paclla, spring	50.8	3710	8.61	81.8	0.00	644	70.0	1.81	252	5.5	928	1.49	1.89	11.7	319	2315	−12.55	−102.8	Na-Cl
15	Llahuar, springs	32.6	2170	8.19	273	37.1	144	3.6	0.00	103	1.76	147	0.71	0.53	9.5	1083	1803	n.d.	n.d.	Ca-Na-SO_4
16		38.1	2500	8.15	300	41. 9	184	3.2	0.00	94.6	1.82	185	0.70	0.59	7.0	1253	2072	−15.78	−118.3	Ca-Na-SO_4
17	Pinchollo, geyser	80.0	337	8.06	46.3	6.7	9.8	5.2	n.d.	45.8	0.29	1.92	0.07	0.00	0.42	151	275	n.d.	n.d.	Ca-SO_4
18		86.0	514	8.37	63.2	10.0	12.9	3.8	0.00	45.8	0.42	1.51	0.18	0.00	1.70	221	360	−14.19	−104.5	Ca-SO_4
19	Pinchollo, springs	35.0	1167	6.66	244	30.6	23.4	3.6	n.d.	772	0.17	2.1	0.00	0.00	4.4	191	1271	n.d.	n.d.	Ca-HCO_3-SO_4
20		30.0	668	8.22	105	24.8	22.0	5.4	n.d.	391	0.50	4.9	n.d.	n.d.	0.11	110	663	n.d.	n.d.	Ca-Mg-HCO_3-SO_4
21		17–18	633	8.27	122	23.3	18.4	4.3	n.d.	387	0.38	2.9	n.d.	n.d.	0.03	158	716	n.d.	n.d.	Ca-Mg-HCO_3-SO_4
22	Hualca Hualca, solfatara	45.0	830	6.98	92.9	23.7	48.6	20.4	n.d.	36.6	0.31	0.38	9.2	0.00	5.4	485	734	n.d.	n.d.	Ca-Na-SO_4
23	Yanque, springs	41.0	1155	7.44	36.0	2.9	269	15.3	n.d.	403	1.11	91.7	0.00	0.20	0.69	229	1049	n.d.	n.d.	Na-HCO_3-SO_4
24		43.1	968	7.55	9.9	0.00	201	10.7	0.37	275	1.37	58.7	0.42	0.23	3.4	157	717	−15.37	−115.6	Na-HCO_3-SO_4
25		59.0	3160	6.68	41.9	0.00	617	33.0	1.20	612	2.6	545	0.71	0.80	5.8	249	2109	−15.65	−120.7	Na-Cl-HCO_3
26	Puye, spring	71.3	3680	6.91	54.5	0.00	759	39.2	1.57	630	2.8	743	0.79	0.93	5.9	235	2470	−15.56	−119.7	Na-Cl-HCO_3
27	Umaru, spring	70.2	6070	6.30	191	4.7	1343	64.8	1.60	550	2.6	1554	1.45	1.58	12.2	538	4263	−16.83	−126.8	Na-Cl
28	Sallihua, spring	47.0	1707	7.00	50.8	3.7	383	33.9	n.d.	400	0.62	356	0.00	0.00	0.55	141	1370	n.d.	n.d.	Na-Cl-HCO_3
29	La Calera, spring	68.9	5494	6.76	137	12.5	1339	75.7	n.d.	848	1.61	1671	0.00	1.64	0.00	311	4398	n.d.	n.d.	Na-Cl-HCO_3
30		68.3	6200	6.69	92.5	0.46	1226	56.2	1.45	590	3.2	1635	0.00	2.1	11.3	308	3926	−17.29	−131.8	Na-Cl
31	La Calera, spring below	49.1	3490	6.73	131	14.1	724	47.6	n.d.	763	0.97	803	0.00	0.77	0.00	239	2724	n.d.	n.d.	Na-Cl-HCO_3
32	La Calera, spring above	65.9	5560	6.64	126	12.2	1330	64.6	n.d.	836	1.31	1578	0.00	0.00	0.00	253	4202	n.d.	n.d.	Na-Cl-HCO_3
33	La Calera, spring below	53.0	4060	6.42	137	12.6	952	57.0	n.d.	793	1.34	1088	0.00	0.00	2.8	241	3285	n.d.	n.d.	Na-Cl-HCO_3
34	Sibayo, spring	48.2	3331	6.92	79.1	6.3	913	20.5	n.d.	1129	1.04	597	0.00	0.00	0.00	316	3061	n.d.	n.d.	Na-HCO_3-Cl
35	Cabanaconde, spring	18.6	335	8.62	25.7	13.6	15.1	2.7	0.00	110	0.32	2.5	0.17	0.06	4.2	69.7	244	n.d.	n.d.	Ca-Mg-Na-HCO_3-SO_4

T_w – water temperature in °C, EC – electrical conductivity in μS/cm, values of ion contents and TDS are in mg/L, isotopic composition of oxygen and hydrogen are in δ unit per mil vs. V-SMOW (Vienna-Standard Mean Ocean Water), n.d. – not determined.

* Measured in laboratory; sample no. as in Table 1 and Fig. 1.

Ca^{2+}, Mg^{2+}, Na^{+}, K^{+}, Li^{+}, B^{+}). The precision and accuracy of field and analytical methods were comparable with those used in our studies.

The AquaChem 4.0.284 software was used to evaluate the geochemical properties of the water samples and to calculate reservoir temperature for thermal waters.

Isotopic analyses (δ^2H, $\delta^{18}O$) of 17 water samples, collected in 2017, were performed in the Stable Isotope Laboratory Institute of Geological Sciences Polish Academy of Sciences. The δ^2H values of studied H_2O were measured using the H-Device peripheral coupled to MAT 253 IRMS (Thermo Scientific) in a dual inlet system. The 1.2 μL of the sample was decomposed in a Cr-filled reactor at a temperature of 850 °C. The isotopic composition of the released H_2 was then measured by IRMS.

For determination of $\delta^{18}O$ in H_2O an equilibration technique was used. The analysis was performed using the GasBench II peripheral device (Thermo Scientific) coupled to MAT 253 IRMS with a continuous He flow. A sample of 0.5 mL of water is equilibrated for 18 h with gaseous CO_2 at 32 °C. Finally, the isotopic composition of equilibrated CO_2 was determined by IRMS. Three international standards were used to calculate the results (VSMOW, USGS 47 and SLAP2 for δ^2H and VSMOW, USGS 47 and W-67400 for $\delta^{18}O$, respectively). The results were reported using δ notation in permill (‰) relative to VSMOW international standard. The analytical precision and measurements accuracy were generally better than ±1‰ for δ^2H and ± 0.12‰ for $\delta^{18}O$, respectively.

Precipitates found at the waters sampling sites were collected separately into plastic bags with strings and sealed boxes. Samples were examined at the Institute of Earth Sciences, the University of Silesia in Katowice. Qualitative chemical composition and mineral habits were investigated with a Philips XL 30 ESEM/TMP scanning electron microscope coupled to an energy-dispersive spectrometer (EDS; EDAX type Sapphire). The phase composition of precipitates was established by X-ray diffraction (XRD). This work involved a Philips PW 3710 diffractometer. Diffraction patterns were interpreted using the X'Pert HIGH-Score Plus software.

Cartographic materials were generated and analyzed using ArcMap 10.2.2 software, copyrighted and licensed by ESRI (http://desktop.arcgis.com/en/). The final layout was created in ArcMap 10.2.2 (http://desktop.arcgis.com/en/) and CorelDRAW 2018 (https://www.coreldraw.com/en/).

4. Results

4.1. Chemical and isotopic ($\delta^{18}O$ and δD) composition of waters

The results of field measurements and laboratory analyses are summarized in Tables 1 and 2. Water temperatures range from 16.1–17.1 °C (No. 5–9) in the cold (Tw < 20 °C) springs of Huambo to 89.0–93.5 °C (No. 10–13) in thermal springs and geysers of Paclla (Fig. 3). Field measurements or estimations show that all thermal springs have discharge not exceeding 10 L/s and most of them less than 5 L/s (Table 1). The only main springs discharging in Huambo river valley have a much larger outflow >100 L/s. Karst springs are draining a large massif of travertines. The pH of the waters is neutral to alkaline and ranges from 6.30 (No. 27) to 8.93 (No. 10). Electrical conductivity (EC) varies from 335 μS/cm (No. 35) to 6200 μS/cm (30). For most thermal springs and geysers, EC exceeds 3000 μS/cm. Values of the total dissolved solids (TDS) among studied thermal waters vary considerably from 275 mg/L (No. 17) to over 4000 mg/L (No. 29, 27, 32, 3; Table 2). TDS of cold waters varies from 244 mg/L (No. 35) to 1287 mg/L (No. 5) (Fig. 3).

The chloride (Cl) content ranges significantly from 0.38 mg/L at Hualca Hualca (22) to 1671 mg/L at La Calera (No. 29; Table 2). All thermal springs generally show high Cl- content, except for waters discharging on the northern slope of extinct volcano Hualca Hualca (No. 17–22). The variations of sulfate content are less pronounced, i.e., from 141 mg/L at Sallihua (No. 28) to 1253 mg/L at Llahuar (No. 16; Table 2). The lowest HCO_3 content (36.6 mg/L) was determined in a stream draining solfatara of Hualca Hualca (No. 22), whereas the highest (1129 mg/L) was at Sibayo (No. 34; Table 2). Several times higher values of the HCO_3 content are recorded in the eastern part of the study area (between Yanque and Sibayo; Fig. 1, Table 2) in comparison to the western cluster located at the bottom of the Colca Canyon.

The sodium (Na) content ranges from 9.8 mg/L at Pinchollo geyser (No. 17) to 1343 mg/L at Umaru (No. 27) and 1339 mg/L at La Calera (No. 29; Table 2). In general, thermal waters discharging in springs located near Canco (No. 1–4) and those in the eastern part of the study area present high Na content (No. 26–34), except for Sallihua (No. 28). On the other hand, those located on the slopes of the Hualca Hualca volcano (No. 17–22) show much lower Na content. The highest values of the magnesium (Mg) content (43.1 mg/L) are recorded at Canco (No. 1;

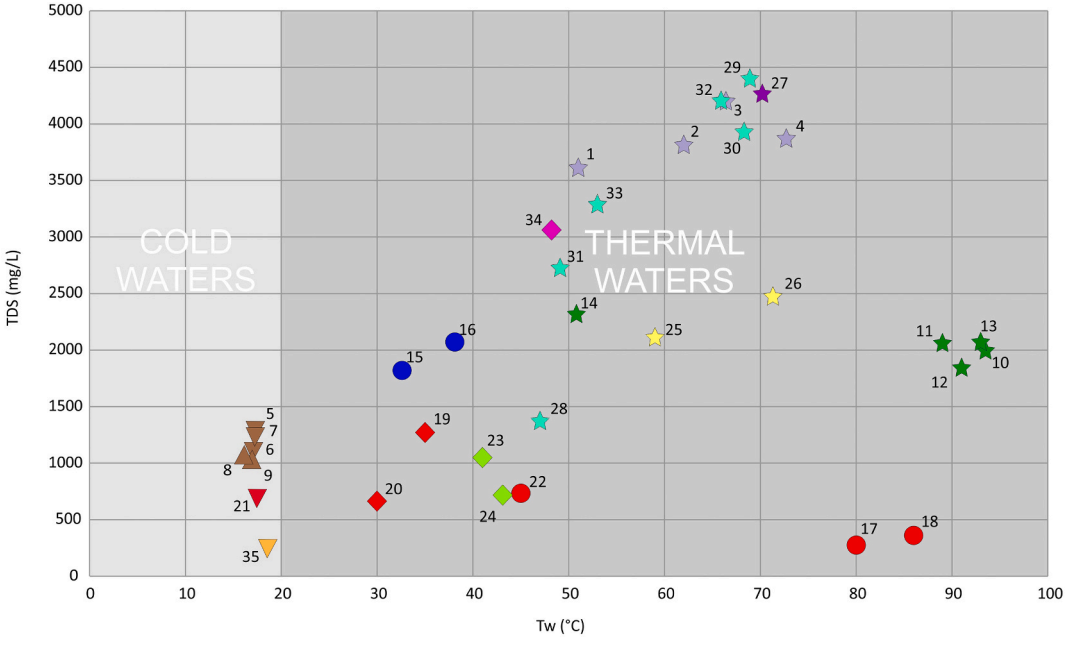

Fig. 3. Plot of TDS against water temperature in the central Colca River basin.

Table 2). Whereas in Paclla (No. 10–14), Yanque (No. 24–25), and Puye (No. 26), this element is absent. Paclla waters (No. 10–14) also show low Ca content (~20–40 mg/L), in comparison to >250 mg/L at Llahuar (No. 15–16) and > 200 mg/L at Canco (No. 1–2). Lithium (Li), i.e., a component related to the hydrothermal solutions, is absent in cold waters (No. 5–9, 21, and 35) and some thermal springs, e.g., Pinchollo geyser (No. 18), Llahuar (No. 15–16). Maximum values reaching >1.8 mg/L are recorded at Paclla (No. 10–14; Table 2).

General chemical composition (major ions) is shown in the Piper diagram (Fig. 4). Additionally, ternary diagrams based on relative concentrations of the three major anions – Cl-SO_4-HCO_3 and Ca-Mg-Na + K (Giggenbach, 1991) are used for cold and thermal waters classification (Fig. 5). The stable isotope oxygen composition of the waters from the study area ranges from −17.29 to −12.44‰ δ^{18}O-VSMOW, and the deuterium ranges from −131.8 to −101.3‰ δD-VSMOW (Table 2, Fig. 6A). All of the thermal water in the study area plot to the right of the local meteoric water line (LMWL, according to Boschetti et al., 2019 equation calculated for northern Chile). Most of the waters cluster close to the global meteoric water line (GMWL, according to Craig, 1961 with modifications by Różański et al., 1993). Cold water discharging in Huambo (No. 6, 8, 9) and thermal water of Pinchollo and Paclla geyser (No. 18 and 10, respectively) plot directly on or very close to the GMWL. In general, the oxygen isotope values are shifted towards higher values than those for precipitations. For thermal waters from springs in Canco (No. 3 and 4) and Paclla (No. 11–14), this shift is significant (Fig. 6A).

4.2. Precipitates at the springs and geysers

Evaporation and oxidation of mineralized thermal waters flowing out of springs, geysers, and solfataras in the Colca River basin lead to mineral precipitation on surrounding rock surfaces, dry plants, and soil. Locally sulfate crust is accumulated up to a few meters thick (Ciesielczuk et al., 2013, 2019) (Fig. 7). Precipitates form coatings, encrustations, and single crystals, mainly white, yellow, or colourless. Dominating mineral phases are Na, NH_4, Ca, K, Al, Mg, Fe sulfates, Ca carbonates, and Na chloride. Native sulfur was also identified (Fig. 8, Table 3). Additionally, quartz, microcline, plagioclase, kaolinite, illite, and mica derived from soil were detected in collected samples.

An abundance (up to 20) of mineral phases precipitates around outflows with the highest temperature and discharge, reaching a maximum of 10 L/s (Table 1). These are the La Calera springs (No. 29–32), Paclla (No. 10–14), and Pinchollo (No. 19–21) geysers and springs. Usually, a few (one to seven) different mineral phases precipitated at Umaru (No. 27), Canco (No. 1–2), Sibayo (No. 34), Sallihua (No. 28), Yanque (No. 23–25), Llahuar (No. 15–16) thermal springs, Huambo (No. 5–6) and Cabanaconde (No. 35) cold springs, and Hualca Hualca (No. 22) solfatara (Table 3).

5. Discussion and conceptual model

5.1. Spatial patterns and processes controlling the chemistry of water

Using Giggenbach's (1991) ternary diagram displaying relative concentrations of major anions (see Fig. 5A), three main hydrochemical

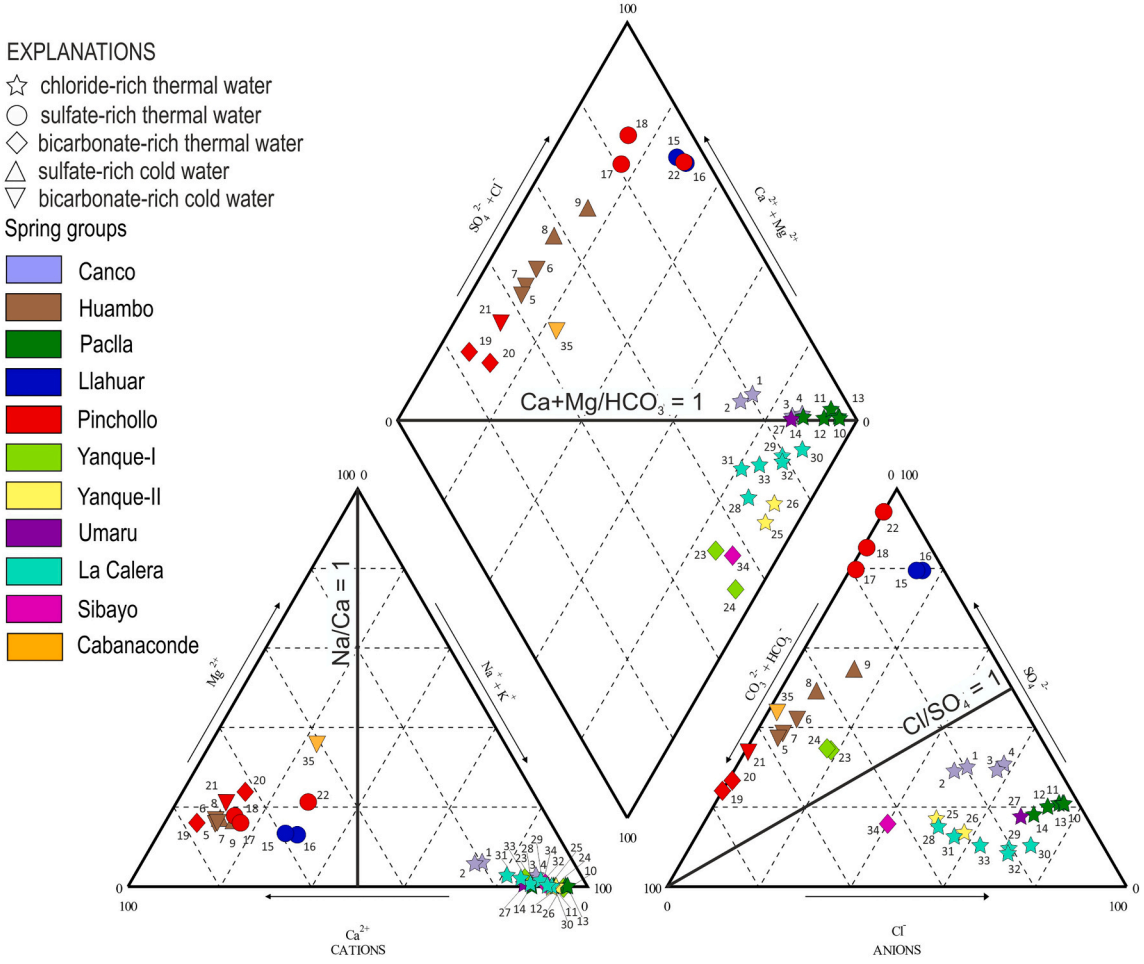

Fig. 4. Piper diagram showing the chemical composition of cold and thermal waters of the central Colca River basin (sample numbers as in Tables 1 and 2).

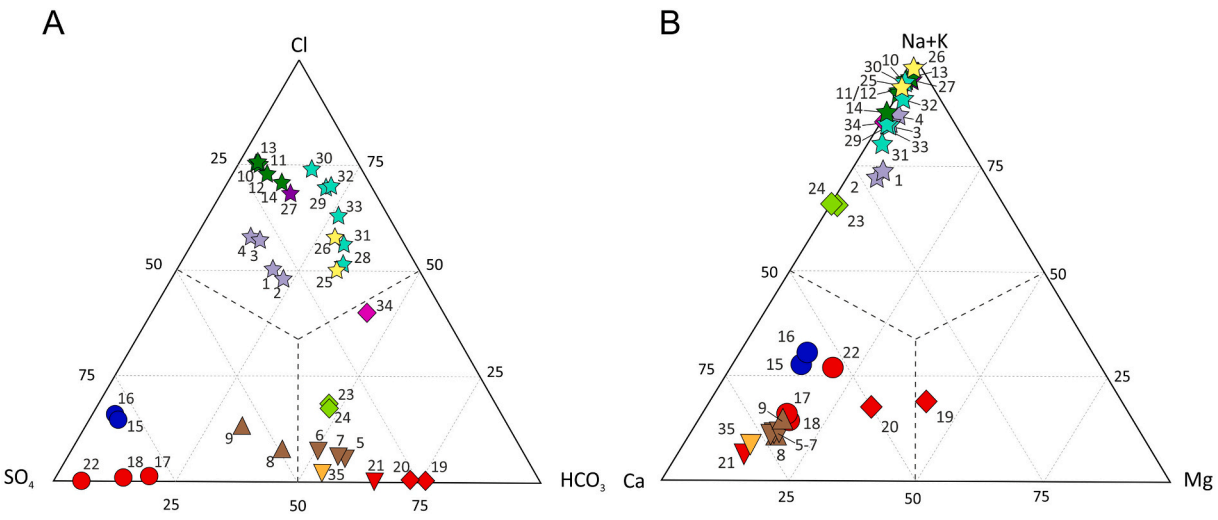

Fig. 5. Relative concentrations of Cl-SO_4-HCO_3 (A) and Ca-Mg-Na + K (B) in waters on the ternary diagram (Giggenbach, 1991).

groups of waters can be distinguished in the study area. Most of the described waters in the Colca River basin belong to the chloride-rich, principally sodium-chloride thermal waters (Fig. 5A, Table 2). Thermal springs located in Paclla (No. 12 and 14), Umaru (No. 27), and La Calera (No. 30) discharge even pure bi-ionic Na—Cl waters. Other springs and geysers at the bottom of the Colca Canyon (i.e., Canco and Paclla) are of Na-Cl-SO_4 type, whereas those in the Colca Valley (Chivay area) are of Na-Cl-HCO_3 type. The thermal spring in Canco (No. 2) appears exceptional within this chloride-rich group discharging multi-ion waters (Table 2).

The second crucial hydrochemical group in the study area includes sulfate-rich waters. These fall into two distinct types - sulfate-rich cold and thermal waters (Figs. 4 and 5A). Ca-SO_4 dominated water discharges in Pinchollo geyser (No. 17 and 18). Other sulfate-rich waters have additional important content of bicarbonate ion (Ca-SO_4-HCO_3 - cold waters of springs No. 8, 9) or sodium ion (Ca-Na-SO_4 - thermal waters of springs No. 15, 16, and 22).

The third group is the bicarbonate-rich waters (Fig. 5A). This group is the most diverse in the Colca River basin. It includes both cold and thermal waters of multi-ion composition: Ca-HCO_3-SO_4 (No. 5–7 and 19), Na-HCO_3-SO_4 (No. 23 and 24), and Na-HCO_3-Cl (No. 34) (Fig. 5 and Table 2). Springs in Pinchollo have a significant content of Mg (Ca-Mg-HCO_3-SO_4 - No. 20 and 21). Although the Piper diagram (Fig. 4) shows that there are no sodium-bicarbonate waters in the study area, the thermal springs in Yanque (No. 23 and 24) and Sibayo (34) are very close to this type of water ionic composition.

5.1.1. *Chloride-rich waters*

Chloride-rich thermal waters (No. 1–4, 10–14, 25–33 on Fig. 1; Tables 1 and 2) is the most significant and uniform hydrochemical group. This is a group of the hottest waters in the studied area (up to 93.5 °C; cf. Table 1). Although relative concentrations of major ions are similar for all chloride-rich waters (Figs. 5A and B), they differ into two more or less distinct hydrochemical and spatial subgroups. The first one is enriched in bicarbonates and is located in the eastern part of the studied Colca River basin - Colca Valley from Yanque to La Calera (Fig. 1). Thermal springs of this area belong to the Chivay geothermal group, according to Steinmüller and Zavala (1997) and Steinmüller (2001). The second subgroup constitutes thermal waters discharging from springs and geysers in Paclla and Canco at the bottom of the Colca Canyon in the western part of the studied area (Fig. 1). Most of the waters discharging in this sector are enriched in sulfates.

The hydrochemical differentiation of the chloride-rich waters, related to the processes in the geothermal reservoir, can be noticed based on specific molecular ratios; these are more like other springs of the Chivay group, where waters are far from the Na/Cl stoichiometric line (Fig. 9A, Table S2). The Na/Cl molar ratio in waters of the Chivay group is >1, which is not related to halite dissolution and can be the result of Na-silicates leaching (e.g., of feldspars or their alteration products) (Chiodi et al., 2015) (Fig. 9A, Table S2). In contrast, thermal waters in Paclla display Na/Cl ratio equal to 1. On the other hand, the Ca/SO_4 ratio in waters in the Chivay geothermal area is close to 1 (Fig. 9B, Table S2), which most probably may result from the secondary dissolution of gypsum in the aquifer. Additionally, salinity origin based on the Cl/Br ratio (Fig. 9C) plots these water samples in the area recognized by Yardley and Bodnar (2014) as characteristic for redissolved evaporites. Based on data from hydrogeochemical monitoring of the Colca River basin performed by INGEMMET (see Table S1), it is possible to consider the origin of solutes involved in shaping the chemistry of chloride-rich thermal waters. Li-Cl-B relative concentrations (Giggenbach, 1992) in three selected thermal spring groups: Puye (No. 26), La Calera (No. 29 and 30), and Paclla (No. 10 and 13), can be used to examine the possible origin of Cl and B in thermal waters (Fig. 10B). The processes related to Li loss or B—Cl absorption may be present in the case of these three thermal springs (Fig. 10B; Giggenbach, 1992; Cortecci et al., 2005). Relative concentrations of SO_4, Mg, and Na situate all the chloride-rich thermal waters on the line of H_2S dissolution in ascending order from La Calera, Puye, and Umaru in shallower Colca Valley to Paclla and Canco in Colca Canyon, but close to the Na corner of the plot (Fig. 10A; Giggenbach, 1992).

Chloride-rich waters show a broad spectrum of $\delta^{18}O$ and δD values (−17.29 to −12.45‰ and − 131.8 to −101.3‰, respectively), with more or less significant positive oxygen shift in relation to LMWL (for northern Chile, after Boschetti et al., 2019; Valdivielso et al., 2021) and GMWL (Fig. 6A). This shift is most significant in the case of Paclla springs and geysers (No. 11–14; up to 1.56‰) and for springs in Canco (No. 3 and 4). One of the geysers in Paclla (No. 10) is discharging the hottest water in the study area (93.5 °C) and has $\delta^{18}O$ and δD values close to those of meteoric water (Fig. 6A). Previous studies (e.g., Field and Fifarek, 1985) proved that thermal waters with high chloride contents represent deep waters of mainly meteoric origin. Such meteoric waters in volcanic areas with high permeability caused by loose tephra, faulting, fracturing, brecciation, and with high topographic gradient as in the Colca River basin, can descend to considerable depths and thereby become heated. After heating up in the geothermal reservoir, these waters can migrate through faults and fracture zones to the discharge zones. Recorded oxygen shift in the Colca Canyon springs may be explained by meteoric waters mixing with magmatic waters in the geothermal reservoir. Still, it

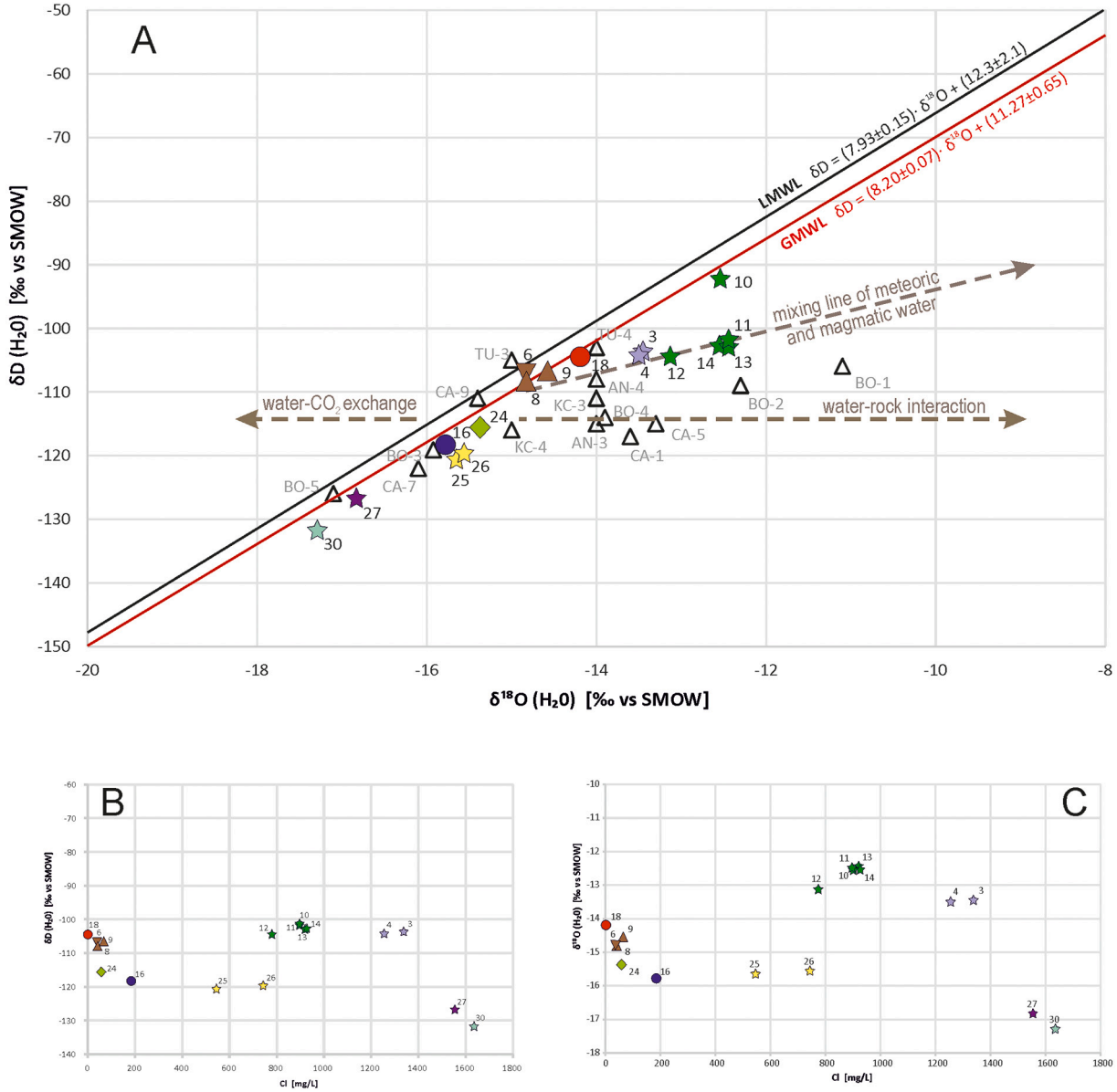

Fig. 6. (A) $\delta^{18}O$ (‰ V-SMOW) vs. δD (‰V-SMOW) plot for cold and thermal waters of the central Colca River basin (colour symbols) and for the Tacna geothermal region in southern Peru (empty triangles with labels referenced in Cruz, 2018); Local Meteoric Water Line (LMWL) after Boschetti et al., 2019; Global Meteoric Water Line (GMWL) after Craig, 1961, with modification by Różański et al., 1993; (B) δD (‰V-SMOW) vs. Cl in mg/L and (C) $\delta^{18}O$ (‰ V-SMOW) vs. Cl mg/L for cold and thermal waters in the study area.

may also result from evaporation, a process that commonly affects thermal waters discharging at the surface (Clark and Fritz, 1997).

The possible input of these magmatic waters or evaporation is more significant in the case of Paclla springs (No. 11–12 and 14) and geyser (No. 13) than in springs in Canco (No. 3 and 4) (Fig. 6A). Isotope composition and recorded positive oxygen shift of thermal waters at the bottom of Colca Canyon is similar to thermal springs Borateras and Calienets (BO and CA on Fig. 6A, respectively) in the Tacna geothermal region in southern Peru (Cruz, 2018). In the case of chloride-rich thermal waters in Paclla and Canco, there is also a more strict relation of both $\delta^{18}O$ and δD with Cl than for water from springs in the Chivay area (Fig. 6B & C). Positive oxygen isotope shift in chloride-rich thermal waters in Colca Valley, less pronounced than in the Colca Canyon, is most probably an effect of the interaction of thermal waters with silicates (water-rock interaction within the geothermal reservoir) (Fig. 6A; Clark and Fritz, 1997; Sacchi et al., 2008).

Precipitates recorded around springs discharging chloride-rich waters are the most diverse and complex mineralogical phases. They are composed mainly of chlorides as halite (Fig. 8-1 A & B), sulfates as gypsum (Fig. 8-1 C), magnesiocopiapite (Fig. 8-1 D), blödite, tamarugite, thenardite, alunogene (Fig. 8-1 E & F), pickeringite (Fig. 8-1 C), and carbonates as calcite and aragonite, trona, and native sulfur. Subordinately, in single springs, the following phases were identified: eugstenite, glauberite (Fig. 8-1 B & G), sideronatrite, boussingaultite, alunite, mercalite, buttlerite, copiapite- copiapite (Mg), coquimbite, halotrichite, jarosite, rhomboclase, rozenite, pertlikite, hexahydrite, picromerite, bassanite, natroxalate, and aphthitalite, alumino coquimbite and polyhalite (Fig. 8-1 A & H) in traces.

5.1.2. *Sulfate-rich waters*

Two small groups of springs and geysers discharge sulfate-rich thermal waters. These are located at the high altitudes (over 4300 m a.s.l.) on the northern slope of Hualca Hualca volcano (Pinchollo geyser, samples No. 17 and 18; Hualca Hualca solfatara, No. 22) and in Llahuar

Fig. 7. Chosen precipitates in the outflows of thermal waters in the central Colca River basin: A – precipitates at the thermal spring in Canco (No. 2); B – precipitates around thermal springs in Paclla (No. 10); C – precipitates at the Pinchollo thermal spring (No. 19); D – native sulfur encrustations at active solfatara vent, the northern slope of Hualca Hualca volcano at 4728 m a.s.l. (No. 22); E – calcite (white streaks) precipitating at the thermal spring above La Calera (No. 32); F –precipitates at the Sibayo thermal spring (No. 34).

at the bottom of Colca Canyon (~2100 m a.s.l.; No. 15 and 16) (Figs. 1 & 5). Waters flowing out of both groups of sulfate-rich thermal springs are of Ca-SO_4 type, some of them enriched in sodium are of Ca-Na-SO_4 type (Fig. 4, Table 2). They reveal a high sulfate indicator (rSO4x100/rCl): >500 in Llahuar and > 5000 on the slope of Hualca Hualca. On the other hand, they show low content of chlorides: (<200 mg/L on the slope of Hualca Hualca) or even very low (<2 mg/L in Llahuar). Lithium was not detected in this type of waters (Table 2).

Significant enrichment of SO_4 in thermal waters in Llahuar (the highest value in the whole study area, >1200 mg/L, very high even if overestimated due to analytical error; Table 2) issued at the bottom of the Colca Canyon may be a result of oxidation processes of H_2S migrating to the surface along with the fractures in the fault zone (see Fig. 10A). Ca/SO_4 ratio display SO_4 excess shown on the diagram in Fig. 9B (see Table S2). Similar but not so clear processes can be observed in the case of Pinchollo geyser, and Hualca Hualca solfatara, where the relative concentration of SO_4 is high (see Figs. 5A and 10A) and native sulfur with alunite and jarosite are common precipitates around the vent (Tables 2 & 3; see also Ciesielczuk et al., 2013). Sulfate-rich thermal waters discharging on the North slope of the Hualca Hualca volcano are plotted in the lower segment of the Cl-SO_4-HCO_3 ternary diagram (Fig. 5A), which according to Giggenbach (1992), may be regarded as characteristic for steam-heated waters. The stable isotope composition (Fig. 6A) of sulfate-rich waters indicates their meteoric origin and lack of Li, and low Cl contents may suggest their shallow circulation. However, it should be emphasized that, unlike other geothermal systems in

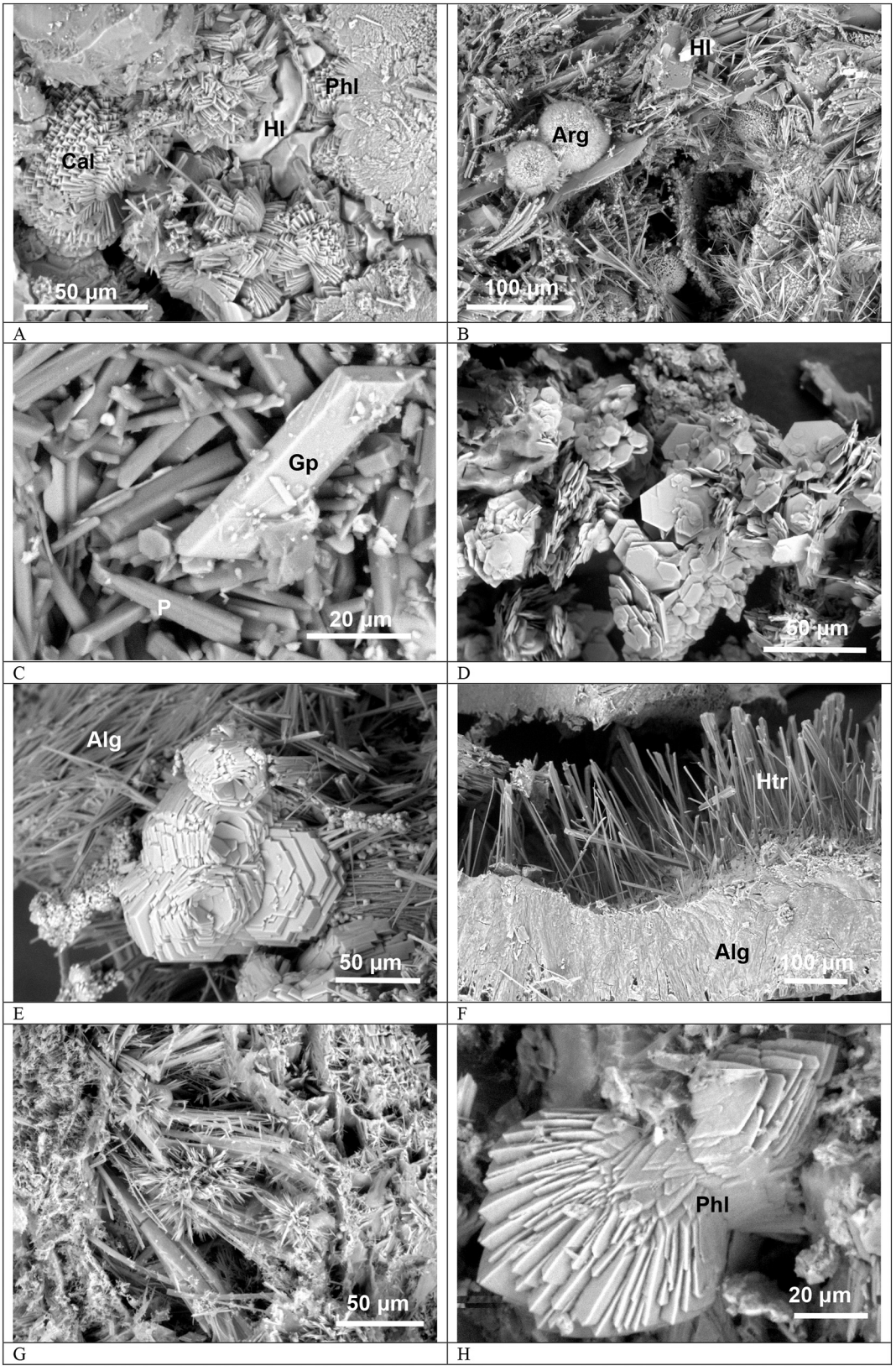

Fig. 8. 1 Precipitates blooming around thermal springs of the chloride-rich water types. A – calcite (Cal), halite (Hl) and polyhalite (Phl) association; B – halite, aragonitic (Arg) spherules and needles of glauberite; C – monoclinic gypsum (Gp) crystal growing on the pickeringite (P); D – magnesiocopiapite; E – aluminocoquimbite on needles of alunogene (Alg); F – needles of halotrichite (Htr) growing on alunogene; G – needles of glauberite; H – polyhalite. A, B, G, H – Canco thermal springs (No. 1–2), C – La Calera (No. 31), D, E, F – Paclla thermal springs (No. 10–14). SEM-BSE images.
2 Precipitates around the springs with sulphate-rich and bicarbonate-rich waters. A – gypsum (Gp) and halite (Hl); B – gypsum crystals; C – gypsum (Gp) and boussingaultite (B); D – bacteria (b) on gypsum crystals; E – copiapite (Cp), alunogene (Alg) and tschermigite (Tsg); F – alunogen (Alg) crystallizing on coquimbite (Cq). A – Llahuar (No. 15–16), B – Cabanaconde (No. 35), C—F – Pinchollo (No. 19–21). SEM-BSE images.

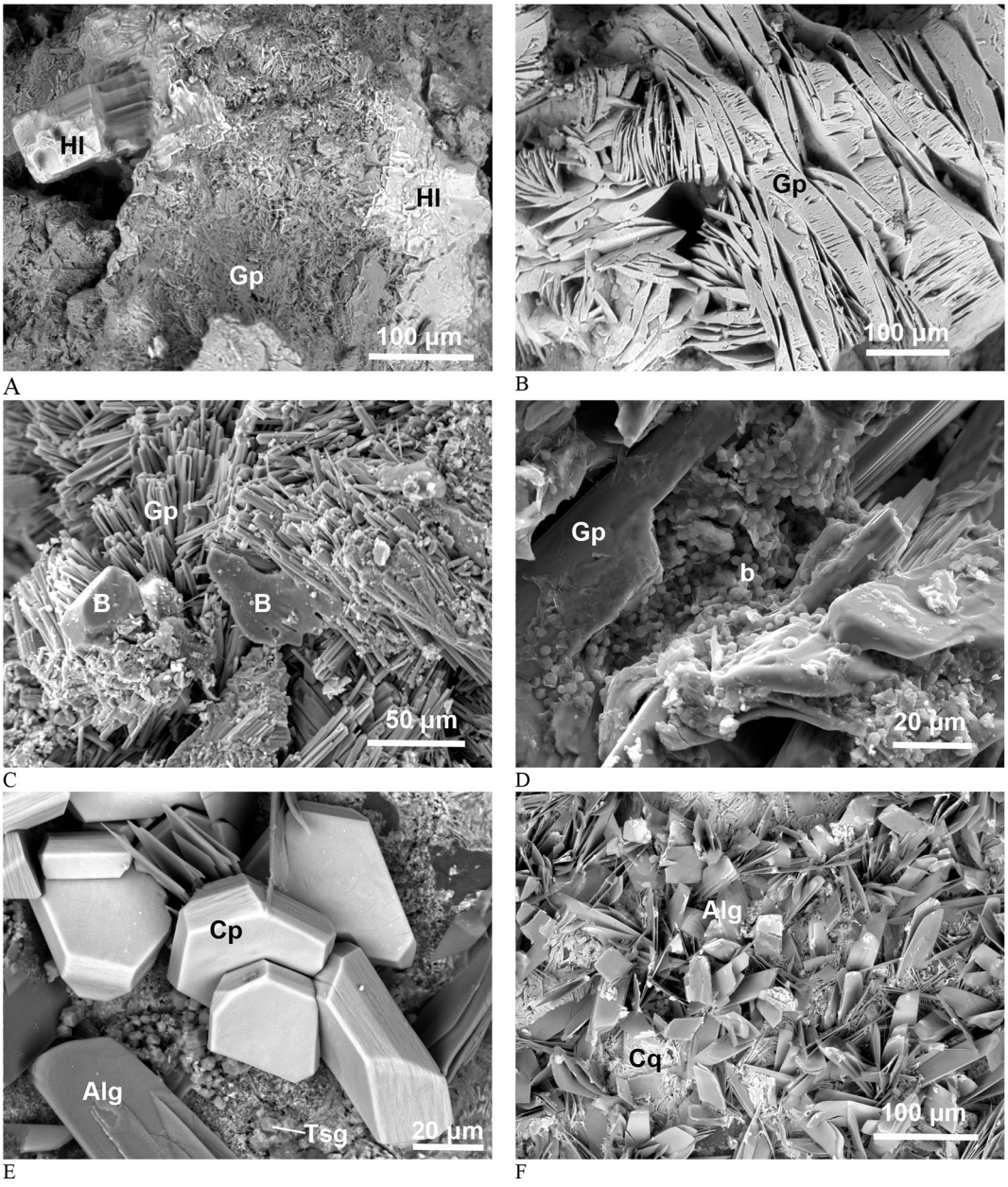

Fig. 8. (*continued*).

Southern Peru, the analyzed sulfate-rich thermal waters are not acidic but alkaline (e.g., Vargas and Cruz, 2010; Cruz, 2018). On the other hand, precipitation of different SO_4 minerals around the outflows of such waters is similar to those reported by Cruz (2018) from Tutupaca acidic thermal springs in the Tacna region (S Peru). Gypsum (see Fig. 8-2 A), alunite, jarosite, and native sulfur are among these similarities. Additionally, other SO_4 minerals, hydrocalumite, blödite, alunogene, and copiapite precipitate around studied springs in the Colca River basin (Table 3; see also Ciesielczuk et al., 2013).

5.1.3. *Bicarbonate-rich waters*

The last relatively small group, i.e., bicarbonate-rich thermal water springs, are represented by Pinchollo (No. 19 and 20), Yanque (No. 23 and 24), and Sibayo (No. 34) (Figs. 1, 3 & 5, Table 2). This group is very diverse in hydrochemical composition: Ca-HCO_3-SO_4 or Ca-Mg-HCO_3-SO_4 in Pinchollo, Na-HCO_3-SO_4 in Yanque, and Na-HCO_3-Cl in Sibayo. The last two groups are located on the peripheries of the Chivay geothermal area, Sibayo, even approximately 20 km upstream from La Calera (Fig. 1), framing bicarbonate-rich waters on the relative concentration Cl-SO_4-HCO_3 diagram (Fig. 5A; Giggenbach, 1992). In other geothermal systems in the Andes, bicarbonate-rich thermal waters are represented by sodium-bicarbonate ones (Steinmüller and Zavala, 1997; Steinmüller, 2001; Vargas, 2010; Vargas and Cruz, 2010; Cruz, 2018).

Low Ca/SO_4 ratio (the lowest among the studied waters) may suggest that dissolved H_2S can play an essential role in shaping the chemical composition of thermal waters in Yanque (sulfates as the third or fourth major ion) (see Fig. 9B), rather than redissolution of evaporites (see Yardley and Bodnar, 2014) recognized for chloride-rich thermal waters of the Chivay geothermal area (Fig. 9C). Conversely, bicarbonate-rich waters in Pinchollo have the highest Ca/SO_4 ratio among the studied waters.

Bicarbonate-rich thermal waters are characterized by a large diversity of mineral precipitation phases, mostly of SO_4 minerals, around the outflows. Ca, Na, Fe, Mg, K, Al, and NH_4-bearing sulfates as gypsum (Fig. 8-2 B—D), boussingaultite (Fig. 8-2 C), thenardite, alunite, alunogene (Fig. 8-2 E & F), copiapite (Fig. 8-2 E), coquimbite (Fig. 8-2 F),

Table 3
Mineral phases in precipitates at the water sampling sites.

Mineral phases	Sample No.														
	27	10–14	1–4	29	32	33	31	28	22	15–16	34	23–24	19–21	5–6	35
	Hydrogeochemical type of water														
	Na-Cl	Na-Cl (12, 14) Na-Cl-SO_4 (10,11,13)	Na-Cl-SO_4 (1, 3, 4) Na-Ca-Cl-SO_4-HCO_3 (2)	Na-Cl-HCO_3	Na-Cl-HCO_3	Na-Cl-HCO_3	Na-Cl-HCO_3	Na-Cl-HCO_3	Ca-Na-SO_4	Ca-Na-SO_4	Na-HCO_3-Cl-	Na-HCO_3-SO_4 (23–24)	Ca-HCO_3-SO_4 (19) Ca-Mg-HCO_3-SO_4 (20,21)	Ca-HCO_3-SO_4	Ca-Mg-Na-HCO_3-SO_4
	Chloride-rich waters								Sulphate-rich waters		Bicarbonate-rich waters				
aluminocoquimbite FeAl $[(SO_4)_3{\cdot}9H_2O$		tr													
alunite $KAl_3[(SO_4)_2\|(OH)_6]$	X								X				X		
alunogene $Al_2(SO_4)_3{\cdot}17H_2O$		X		X			X		X				X		
aphthitalite $(K,Na)_3Na(SO_4)_2$		tr													
aragonite $CaCO_3$	X		X												
bassanite $CaSO_4{\cdot}0.5H_2O$		X													
blödite $Na_2Mg(SO_4)_2{\cdot}4(H_2O)$		X		X		X			X		X	X			
boussingaultite $(NH_4)_2Mg$ $[SO_4]_2{\cdot}6H_2O$		X											X		
butlerite $Fe(SO_4)(OH)_2{\cdot}2H_2O$							X								
calcite $CaCO_3$	X	X	X		X			X			X			X	X
copiapite $FeFe_4[(SO_4)_6\|$ $(OH)_2{\cdot}20H_2O$							X		X				X		
coquimbite $Fe_2^{3+}[SO_4]_3{\cdot}9H_2O$				X									X		
eugstenite Na_4Ca $(SO_4)_3{\cdot}2H_2O$			X												
glauberite $Na_2Ca(SO_4)_2$		X													
gypsum $CaSO_4{\cdot}2H_2O$		X		X		X	tr		X	X	X	X	X		X
halite NaCl		X	X	X		X		X		X	X	X			
halotrichite $Fe^{2+}Al_2(SO_4)_4$		X													
hexahydrite $MgSO_4{\cdot}6H_2O$						X									
hydrocalumite Ca_2Al $(OH)_6[Cl_{1-x}(OH)_x]$ $\cdot 3H_2O$										X					
jarosite $KFe^{3+}{}_3(SO_4)_2(OH)_6$				X					X				X		
magnesiocopiapite $MgFe$ $(SO_4)_6(OH)_2{\cdot}20(H_2O)$		X		X			X								
mercalite $KHSO_4$			X												
mohrite $(NH_4)_2Fe$ $[SO_4]_2{\cdot}6H_2O$													X		
monohydrocalcite $CaCO_3{\cdot}H_2O$															X
native sulfur S_8		X		X					X						
natroxalate $Na_2C_2O_4$												X			
pertlikite $K_2(Fe^{2+}, Mg)_2$ $Mg_4Fe^{3+}{}_2Al(SO_4)_{12}{\cdot}18$ (H_2O)				X											
pickeringite $MgAl_2[SO_4]_4{\cdot}22H_2O$		X		X			X						X		
picromerite K_2Mg $(SO_4)_2{\cdot}6H_2O$						X									
polyhalite K_2Ca_2Mg $(SO_4)_4{\cdot}2H_2O$			tr												
rhomboclase (H_5O_2) $Fe^{3+}(SO_4)_2{\cdot}2(H_2O)$		tr		X											
rozenite $Fe[SO_4]$ $\cdot 4H_2O$		X										tr	X		
sideronatrite $Na_2Fe(SO_4)_2{\cdot}(OH)$ $3(H_2O)$						X									
tamarugite $NaAl(SO_4)_2{\cdot}6$ (H_2O)		X		X		X									
thenardite Na_2SO_4				X				X			X	X	X		
trona $Na_3(CO_3)_2(HCO_3){\cdot}2$ (H_2O)								X			X				
tschermigite $(NH_4)Al$ $[SO_4]_2{\cdot}12H_2O$													X		
voltaite $K_2Fe_5^{3+}[SO_4]_4{\cdot}18H_2O$ - voltaite (Mg)													X		

X – identified by XRD, tr- traces; sample no. as in Table 1 and Fig. 1.

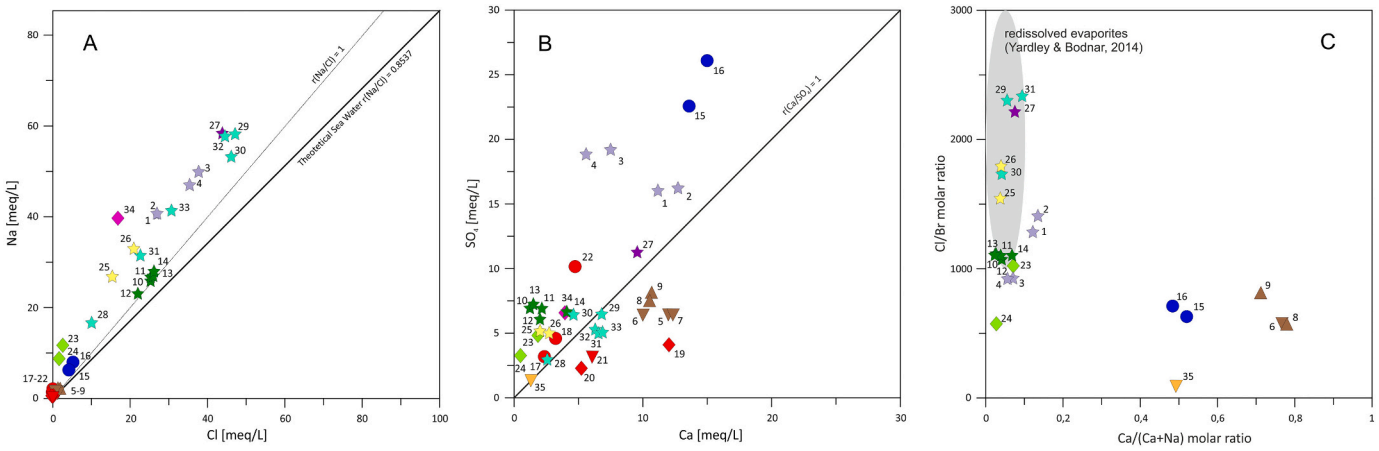

Fig. 9. Relationships between Na and Cl (A), Ca and SO_4 (B), and the proportion of Ca to Na in crustal brines and the origin of their salinity, as indicated by Cl/Br ratios (C) for waters of the central Colca River basin.

jarosite, rozenite, voltaite-voltaite (Mg), pickeringite, mohrite and tschermigite (Fig. 8-2 E) were identified. Calcite and monohydrocalcite as the only carbonate minerals were found. The activity of sulfur-ophilous bacteria was also documented on the precipitate sample from Pinchollo (Fig. 8-2 D).

5.1.4. Cold waters

Cold waters (Tw < 20 °C) of the central Colca River basin represent three different spring areas in the Colca Canyon and Valley. They appear at higher altitudes: 3347–3362 m a.s.l. in Huambo (No. 5–9), 3450 m a.s.l. in Cabanaconde (No. 35) and 4395 m a.s.l. in Pinchollo (No. 21) (Fig. 1, Tables 1 & 2). Two (No. 8 and 9) can be considered sulfate-rich cold waters, and the others as bicarbonate-rich cold waters (Figs. 4 & 5). Contrary to the Huambo springs (No. 4–7) draining fissure-karst system within the large travertine cover, which are the largest in the area (discharge >100 L/s), the two others (No. 21 and 35) located on the slope of Hualca Hualca display little outflow. The water temperature reflects the average air temperature for the elevation of the spring's location. Relatively high TDS (>1000 mg/L) and significant concentrations of sulfates in waters draining the carbonate massif, which on the other hand have a $\delta^{18}O$ and δD composition of meteoric waters are characteristic for the sulfate and bicarbonate cold waters of Huambo. Direct observations of gypsum pseudomorphoses after calcite in caves developed in travertines at the groundwater level suggest that these are enriched in SO_4 due to the oxidation of H_2S in the aquifer and the dissolution of secondary gypsum (Tyc et al., 2021).

The central Colca River basin lacks typical bicarbonate waters (see Figs. 4 & 5) and is characterized by the small share of carbonates among the identified precipitates around studied springs. This is largely the result of a relatively small contribution of carbonate rocks, occurring only locally in the form of travertine covers or limestones of the Arcurquina and the Ashua Formations in the western part of the study area (Fig. 1B). Previous geothermal studies in the Peruvian Andes (e.g., Steinmüller and Zavala, 1997; Steinmüller, 2001) reported travertines as dominant surface precipitates of thermal springs. Therefore, the neutral and alkaline pH of most Colca River basin thermal springs is related to the presence of non-carbonate alkalis (according to Piper's classification of waters, Piper, 1944; see Figs. 4 & 5).

5.2. Reservoir temperatures

The analytical data for the fluid discharges presented in this study may be used to evaluate the temperature path with depth that may be expected in the geothermal system in the central Colca River basin. For this purpose, we used a ternary diagram displaying the concentration of Na, K, and Mg in the triangle vertex, proposed by Giggenbach (1988) (Fig. 11), taking into account the fact that this diagram does not necessarily reflect the reservoir temperature (e.g., see discussion in Romano and Liotta, 2020). The reservoir temperatures were estimated using Na—K geothermometers proposed by Giggenbach (1988), Verma and Santoyo (1997), Can (2002), and Santoyo and Díaz-González (2010) (see Table S3).

The Na-K-Mg ternary diagram allows classifying thermal waters in the Colca River basin into immature, partially, or fully equilibrated waters. Waters of thermal springs and geysers in Pinchollo (No. 17–20), Hualca Hualca (No. 22), and Llahuar (No. 15 and 16) are immature. These immature waters are of sulfate-rich (Ca-SO_4 or Ca-Na-SO_4) or bicarbonate-rich type (Ca-HCO_3-SO_4 or Ca-Mg-HCO_3-SO_4). For the samples plotting far into the immature waters sector of the diagram, the application and interpretation of any cation geothermometers are problematic (Giggenbach, 1988). In this case, the temperatures reported for sulfate-rich and some calcium-bicarbonate thermal springs and geysers must be interpreted with caution (see Table S3).

Most of the thermal waters studied are plotted in the partial equilibrium - dilution sector of the diagram (Fig. 11). Almost all samples are located on the narrow range of reservoir temperatures (180–200 °C, see Table S3 and Fig. 11) and along the line of increasing equilibration (lowering dilution by meteoric/groundwaters). They are chloride-rich thermal waters (Na—Cl, Na-Cl-HCO_3, or Na-Cl-SO_4) of the Chivay region (No. 25–33) and Canco springs (No. 1–4) at the bottom of the Colca Canyon (see Fig. 1). In this partially-equilibrated group, waters are discharging in springs of the Yanque (No. 23 and 24) and Sibayo (No. 34), which give-off bicarbonate-rich waters with high sodium content (Na-HCO_3-SO_4 and Na-HCO_3-Cl, respectively). Chloride-rich waters in Sallihua (No. 28) spring are partially equilibrated, but the reservoir temperature for this water is higher than 220 °C. Another exception is bicarbonate-rich water discharge in Sibayo (No. 34) with an estimated equilibration temperature of ~140 °C. Sodium-chloride waters discharging in Puye spring (No. 26) and Paclla springs and geysers (No. 10–14) are fully equilibrated with primary and secondary minerals in the geothermal reservoir (Fig. 11). Waters discharging in Paclla is also the hottest issued in the studied area. However, the estimated temperature of equilibration with reservoir rocks in case of Puye is within the limits of values obtained for the remaining waters of the Chivay region (~185 °C), reservoir temperature in case of Paclla is different, reaching ~240 °C (see details in Table S3).

5.3. Thermal waters and active faults

Spatial distribution of studied thermal springs in the Colca River basin, especially those in Paclla (No. 10–14), Llahuar (No. 15–16), Yanque (No. 23–25), Puye (No. 26), Umaru (No. 27), and Sallihua (No.

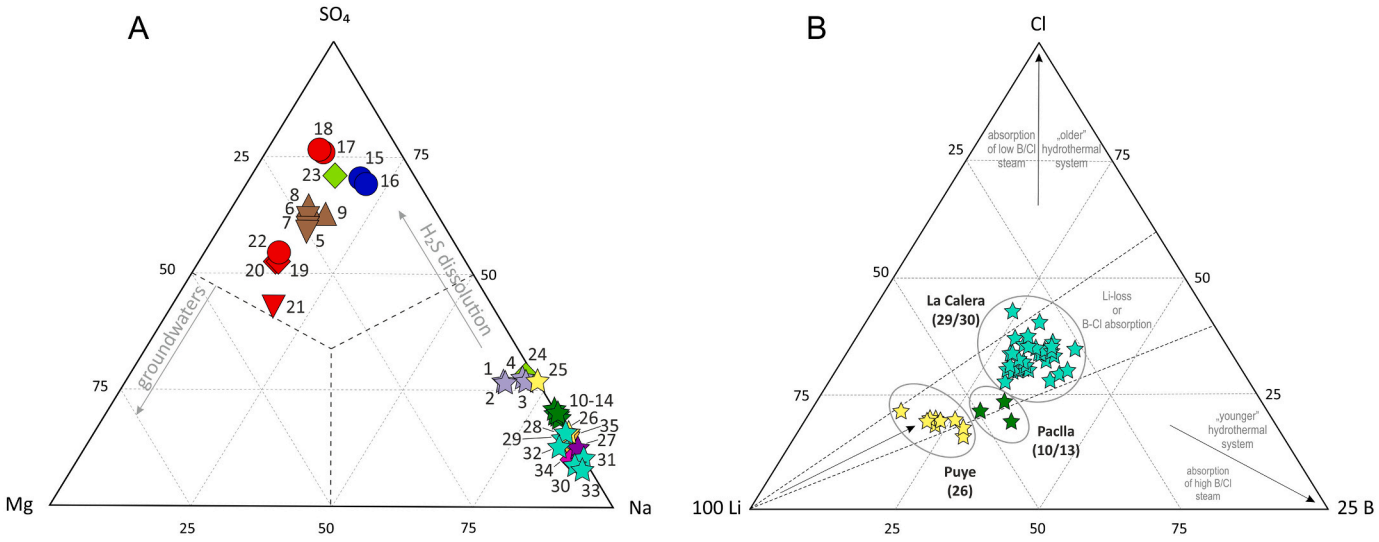

Fig. 10. SO_4-Mg-Na ternary diagram for cold and thermal waters (A) and Li-Cl-B ternary diagram for waters of selected thermal springs (B) of the central Colca River basin.

28), and those located on the northern slopes of Hualca Hualca volcano (No. 17–22) show a clear correlation with crustal normal and strike-slip faults (see Fig. 12) recorded in the field (e.g., Ciesielczuk et al., 2013; Gaidzik et al., 2020), mapped on a neotectonic map (Benavente et al., 2017) and/or derived from focal mechanisms as seismo-lineaments (Gaidzik and Więsek, 2021). Worldwide examples prove that active faults and related fault-fracture network may play a crucial control in thermal water upflow/outflow, mainly promoting the advection of fluids and heat, e.g., Alpine Fault, New Zealand (Townend et al., 2017), Los Geysers Field in the Trans-Mexican Volcanic Belt, Mexico (González-Guzmán et al., 2019), Liquiñe-Ofqui Fault System and Andean Transverse Faults in South Volcanic Zone, Chile (e.g., Cortecci et al., 2005; Pérez-Flores et al., 2016; Roquer et al., 2017; Wrage et al., 2017), Nekor fault and other active structures in Marocco (Tassi et al., 2006), and the Sardinian Rift-Campidano Graben, Italy (Sacchi et al., 2008).

Thermal springs at the bottom of the Colca Canyon in Paclla (No. 10–14) and Llahuar (No. 15–16) extend parallelly along the 80 km long and NW-striking oblique-slip active Chachas-Cabanaconde-Patapampa Fault System (Fig. 12). The northernmost segment of this fault reaches the eastern flanks of the Valley of Volcanoes and, after a stepover, is replaced by active Andagua and Taucas Faults of the same orientation. The south-eastern segments were reactivated in 2013 with earthquakes of $M > 5$ and produced coseismic fissures and surface rupture of 15 cm to the north of the Pinchollo geyser (No. 17–18; Fig. 12; Benavente et al., 2017).

Northern slopes of the Hualca Hualca volcano are cut by a complex active faults network represented by generally W-striking segments of at least three systems; from the north, these are Chachas-Cabanaconde-Patapampa Fault System, Solarpampa-Puye Puye-Pillo Fault System, and Pungo-Hornillo Fault System (Fig. 12). The trace of the second system coincides with the location of the Pinchollo geyser (No. 17–18) and adjacent springs (No. 19–21; Fig. 12; see also Ciesielczuk et al., 2013). Its activity is corroborated by up to 40 m high fault scarps, sagponds, deformation of the drainage system, displacements of Holocene volcanic formations, and alluvial deposits (e.g., Sebrier et al., 1985; Benavente et al., 2017). This fault system is also considered a source of shallow earthquakes of $M > 5$ with normal focal mechanisms that affected the Cabanaconde town (e.g., Antayhua et al., 2002). Scaling relationships proposed by Wells and Coppersmith (1994) and mapped traces suggest potential earthquakes of maximum magnitudes exceeding 7.0 for this fault (Gaidzik and Więsek, 2021). The most elevated spring (No. 22), on the other hand, is located where the W-striking normal Pungo-Hornillo Fault System cross-cut the Hualca Hualca north slope (Fig. 12).

Springs in Yanque (No. 23–25), Puye (No. 26), Umaru (No. 27), and Sallihua (No. 28) are located at the intersection, or reasonably close, of the Yanque Fault and Ichupampa Fault with the Colca Valley (Fig. 12). These two structures form the central part of the regional active NW-striking sinistral Río Cotahuasi-Ichupampa-San Juan de Tarucani Fault System, stretching over 240 km from the upstream section of the Ocoña River in the NW to the northern slopes of the Ubinas Volcano in the SE segment. Recent activity of this structure is corroborated by the existence of fault scarps, deformations observed in the alluvial and lacustrine deposits in the Colca Valley, anomalies in the drainage system, etc. (Benavente et al., 2017), and most recently (14.08.2016) by an earthquake of M 5.3 that resulted in 4 fatalities, >100 buildings collapsed and numerous mass movements and infrastructure deformations (Delgado et al., 2016).

The location of the cold water spring (No.35) in Cabanaconde appears to coincide with the trace of the active normal W-striking Trigal Fault System (Fig. 12). Pronounced in the morphology scarps several meters high together with sagponds, displacements of Holocene

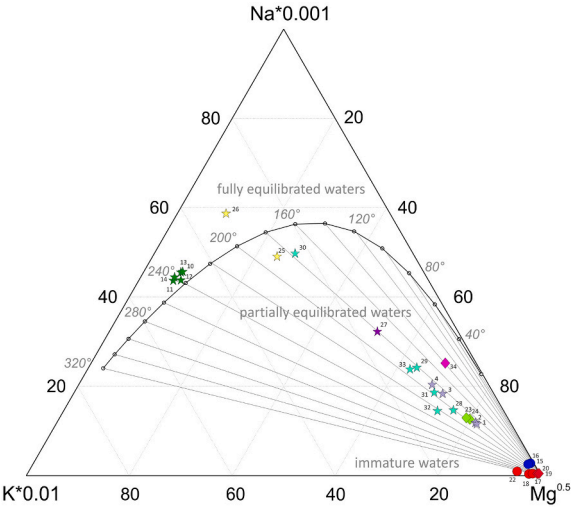

Fig. 11. Na-K-Mg relations on the ternary diagram (Giggenbach, 1988) for thermal waters of the central Colca River basin.

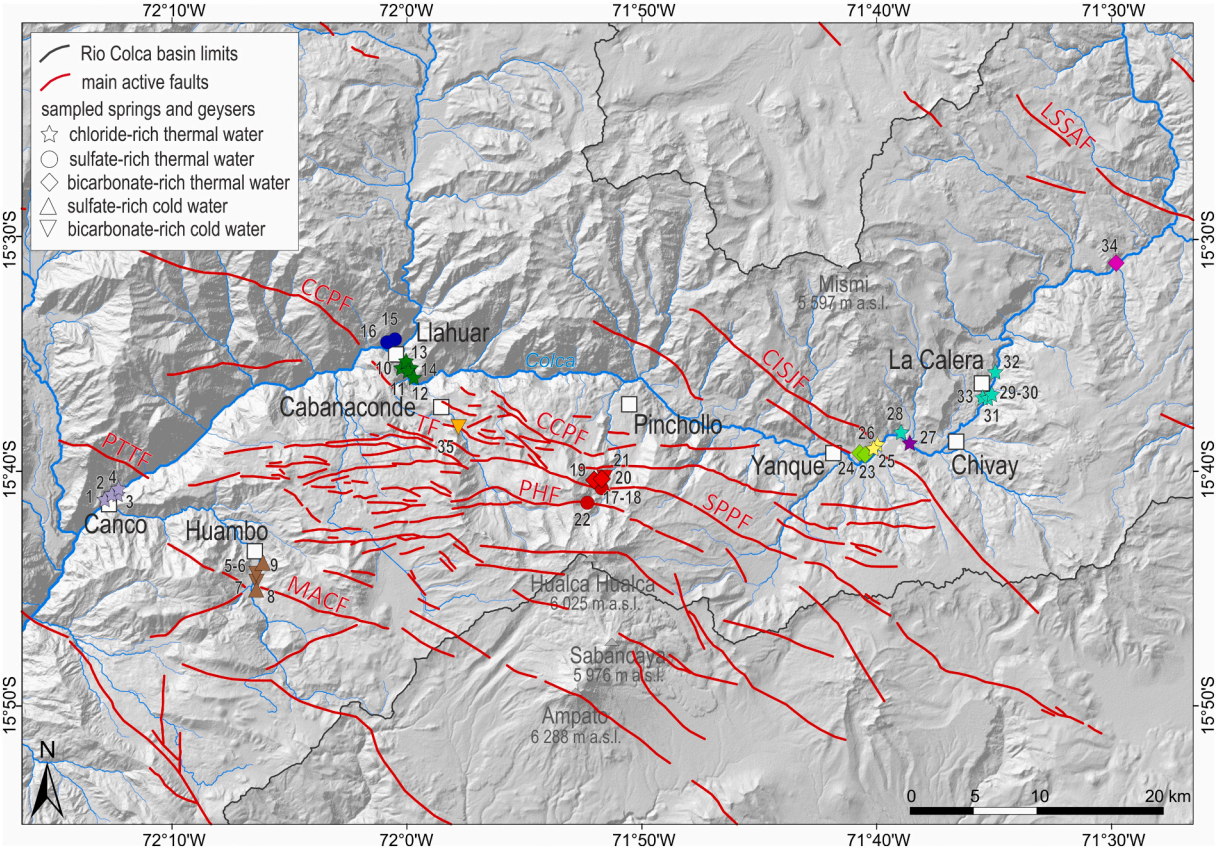

Fig. 12. Studied thermal springs (No. 1–35) in the central Colca River basin versus main active faults (according to Benavente et al., 2017): CCPF - Chachas-Cabanaconde-Patapampa Fault, SPPF - Solarpampa-Puye Puye-Pillo Fault, PHF - Pungo-Hornillo Fault, CISJF - Río Cotahuasi-Ichupampa-San Juan de Tarucani Fault, TF - Trigal Fault, PTTF - Pallca-Tunupacha-Toro Fault, MACF - Mucurca-Ampato-Casablanca Fault, LSSAF - Llacmapampa-Sibayo-San Antonio de Chuca Fault.

deposits, deformation of the drainage system, and small features observed in the palaeoseismological trench (e.g., slumps, mud volcanoes, sismites, deformed lamination, and flame structures) corroborate the Holocene activity of this 20 km long faults that are assumed to produce earthquakes of M > 6 (Sebrier et al., 1985; Benavente et al., 2017).

The relation between thermal springs and active faults is less pronounced in other sectors, although their potential correlation cannot be neglected. Springs in Canco (No. 1–4) do not coincide with any known active fault trace. However, their location suggests a possible relationship with one of the following fault systems: WNW-striking normal Pallca-Tunupacha-Toro Fault System located c. 2 km to the north and/or NW-striking reverse Mucurca-Ampato-Casablanca Fault System that ends some 4 km to the SE, but its possible extension (as blind fault) would point out exactly the location of Canco springs (see Fig. 12). This is even more likely as the trace of this fault is generally not well-constrained, and its visibility in the topography is limited (Benavente et al., 2017). Moreover, the Mucurca-Ampato-Casablanca Fault also appears to be potentially related to some of the cold springs in Huambo (No. 5–9).

The most-eastern spring in Sibayo (No. 34), even though not exactly on a fault trace, could be related with the reverse NW-striking Llacmapampa-Sibayo-San Antonio de Chuca Fault System (Fig. 12) that at this segment is regarded as a tectonic border between Western Cordillera and Altiplano (Benavente et al., 2017).

The most puzzling are thermal springs in La Calera (No. 29–33) that do not correlate with any known active fault system, nor do they appear in reasonable proximity (see Fig. 12). The closest is the NW-striking sinistral Río Cotahuasi-Ichupampa-San Juan de Tarucani Fault System, located ~7–8 km to the south (Fig. 12). Whether springs in La Calera may be related to some structures originated by these sinistral faults, we cannot neglect that another unrecognised or secondary fault-fracture system provides conduits for these springs. Located here, thick (>100 m) and vast (> 10 km^2) Pleistocene lava valley fill might also occult any traces of local faults that might not be seismogenic but still provide paths for fluids and heat (Fig. 12).

5.4. Conceptual model

The hydrogeochemical and isotopic (δD and $\delta^{18}O$) characteristics of studied waters, estimated reservoir temperatures, associated precipitates in the vicinity of thermal springs, and relationships with tectonic and volcanic activity indicate a complex geothermal system in the Colca River basin. The presence of an active magmatic chamber of the Ampato-Sabancaya Volcanic Complex at a depth of 12–15 km below the ground surface (Boixart et al., 2020) appears to be crucial for the presence of the geothermal reservoir in this region (Fig. 13). The location of the vast majority of studied thermal springs along active W- to NW-trending normal and strike-slip crustal faults suggests strong structural control of the geothermal system (Fig. 12). Using fractures and faults as migration paths, pressured magmatic fluids and gases (steam) tend to ascend from the heat source to the geothermal reservoir (Fig. 13). Active faults provide open pathways for the circulation of such fluids (Barnes et al., 1978). While rising to the surface, these fluids may undergo phase separation, mixing with meteoric waters and chemical re-equilibration leading to variable chemical and isotopic composition at the surface (e.g., Minissale, 2004; Pérez-Flores et al., 2016; González-Guzmán et al., 2019). In the Colca River basin, these processes, together with a considerable gradient of pressure owing to local relief (c. 4000 m between the bottom of the Colca Canyon in Canco and the volcano peaks)

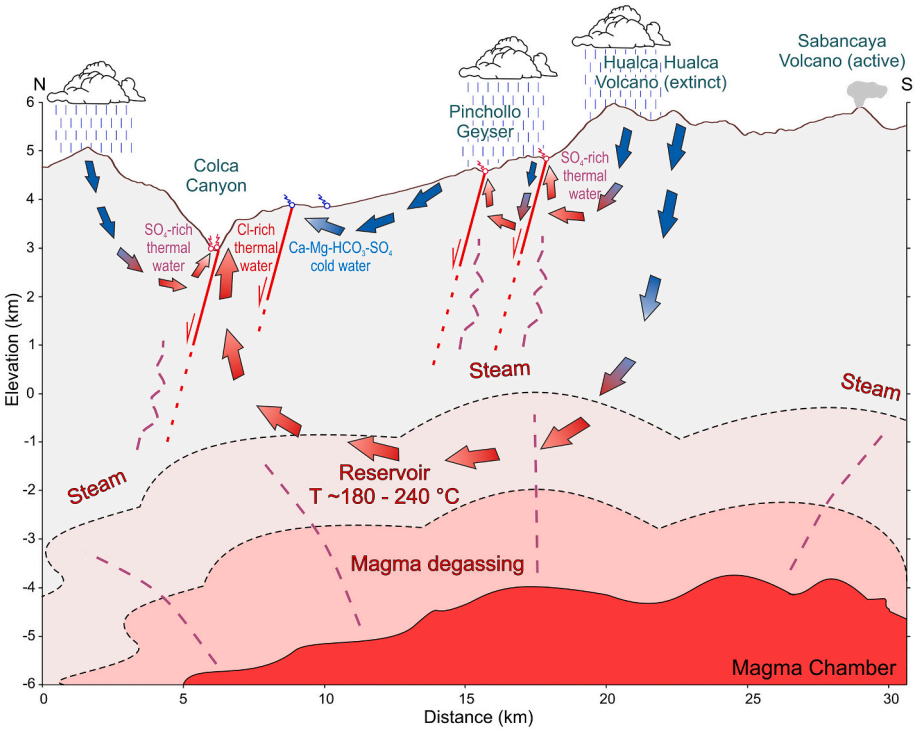

Fig. 13. Conceptual model of the central Colca basin geothermal system – the Colca Canyon sector of the system. Depth of the magma chamber beneath the Hualca Hualca volcano according to Boixart et al. (2020). See text for explanation.

and deep incision in the Canyon, led to differentiation of the water circulation regime and division of thermal waters into three discussed earlier groups. These are: (1) regional, deep circulation of meteoric waters reaching geothermal reservoir and mature through water-rock interaction, and mixing with magma waters or/and due to evaporation – chloride-rich, mostly sodium-chloride thermal waters (No. 1–4, 10–14, 25–33, see Fig. 13), and very diverse in hydrochemistry thermal waters resulted in the shallow circulation of meteoric waters enriched with sulfates (2) (No. 15–18, 22) or with bicarbonates (3) (No. 19–20, 23, 24, 34) The sulfate-rich waters are shallow meteoric waters heated by ascending gases, and they form an independent group referring to the local water circulation (Fig. 13). The bicarbonate ones are the intermediate group of meteoric waters partially equilibrated in a geothermal reservoir on its periphery or shallower depth and more similar to chloride-rich waters (No. 23, 24, and 34), or additionally enriched with SO_4 and more similar to sulfate-rich waters (No. 19 and 20). Faults play a significant role in locating the outflows of various types of water, which on the one hand in compressed sections might act as a barrier to meteoric waters infiltrating the massif (e.g., Angelone et al., 2005), and on the other hand, in tensional settings provide access to hydrothermal solutions, gases and heated waters (e.g., Barnes et al., 1978; Tassi et al., 2006; Pérez-Flores et al., 2016).

6. Conclusions

Thermal waters in the central part of the Colca River basin discharge in springs and geysers draining Jurassic-Cretaceous to Quaternary sedimentary and volcanic formations at variable elevations ranging from 1380 to 2140 m a.s.l. at the Colca Canyon floor, to 3300–3800 m a.s.l. at the Colca Valley floor and 4330–4750 m a.s.l. on the northern slopes of the Hualca Hualca volcano. Our results indicate a heterogeneous and complex thermal system with contrasting hydrogeochemical and physical properties, variable isotope composition, different reservoir temperatures, and associated precipitates around thermal springs.

Processes controlling water chemistry are related to the location of the magmatic chamber of the Ampato-Sabancaya Volcanic Complex (ASVC) and tectonic structures that allow complex interactions of meteoric waters with geothermal reservoir and spatial differentiation of thermal water types in that area.

Chloride-rich thermal waters are the dominant type in the central Colca River basin. These are discharging at the bottom of the Colca Canyon (No. 1–4, 10–14) and Colca Valley (No. 25–33), and their overall geochemical spectrum results in highly variable mineral phases precipitating at the outflows. Chloride-rich waters are partially equilibrated, except for Paclla springs and geysers (No. 10–14) and spring in Puye (No. 26), discharging waters fully equilibrated with the reservoir rocks. The reservoir temperature, estimated by Na/K geothermometry, ranges between 180 and 200 °C, up to ~240 °C in Paclla. Chloride-rich, mainly sodium chloride thermal waters are of meteoric origin but mature within the geothermal reservoir due to water-rock interaction, mixing with magmatic waters or/and due to evaporation processes.

The sulfate-rich waters (No. 15–18, 22) are shallow meteoric waters heated by ascending gases, and they form an independent group referring to the local water circulation, often controlled by tectonic barriers. The bicarbonate ones are the intermediate meteoric waters, divided into two hydrochemical groups: waters partially equilibrated with reservoir rocks and more similar to chloride-rich waters (No. 23, 24, and 34) or enriched with SO_4 more similar to sulfate-rich waters (No. 19 and 20).

The phase composition of precipitates accompanying thermal springs in the central Colca River basin reflects their long-term formation under several overlapping processes. The data obtained is insufficient for precise modelling and explanations and needs further investigation.

All studied thermal springs, except springs in La Calera, show a clear spatial correlation with active and seismogenic crustal W- to NW-tracing normal and strike-slip faults. These might act as a barrier to infiltrating meteoric waters, e.g., on the northern slopes of the Hualca Hulaca volcano. Most importantly, however, these tectonic structures provide pathways to hydrothermal solutions and gases assisting in meteoric water heating. On the other hand, the tectonic structures provide

passages for heated waters that are pressurized by lithostatic load to ascend to the surfaceat the bottom of the Colca Canyon or Colca Valley.

Declaration of Competing Interest

The authors declare that they have no known competing financial interests or personal relationships that could have appeared to influence the work reported in this paper.

Supplementary data to this article can be found online at https://doi.org/10.1016/j.jvolgeores.2022.107513.

Acknowledgments

This research was funded by National Science Centre (Poland), grant No 020/39/B/ST10/00042, and Institute of Earth Sciences, University of Silesia, Poland. For the purpose of Open Access, the authors have applied a CC-BY public copyright licence to any Author Accepted Manuscript (AAM) version arising from this submission. We want to thank W.E. Krawczyk for her inspiration for water sample collection, S. Jakóbczyk-Karpierz for her help in data analyses, T. Krzykawski for conducting XRD analyses. We are grateful to the local communities of the Colca drainage basin for kindly giving us access to work and for help in the field. The authors are grateful for the thorough, helpful work of Tobias P. Fischer (Editor), Franco Tassi and another anonymous reviewer, which comments and suggestions greatly improved the article.

References

Angelone, M., Gasparini, C., Guerra, M., Lombardi, S., Pizzino, L., Quattrocchi, F., Sacchi, E., Zuppi, G.M., 2005. Fluid geochemistry of the Sardinian Rift-Campidano Graben (Sardinia, Italy): fault segmentation, seismic quiescence of geochemically "active" faults, and new constraints for selection of CO2 storage sites. Appl. Geochem. 20 (2), 317–340. https://doi.org/10.1016/j.apgeochem.2004.08.008.

Antayhua, Y., Tavera, H., Bernal, I., 2001. Análisis de la actividad sísmica en la región del volcán Sabancaya (Arequipa). Bol. Soc. Geol. Peru 91, 55–68.

Antayhua, Y., Tavera, H., Bernal, I., Palza, H., Aguilar, V., 2002. Localizacion hipocentral y caracteristicas de la fuente de los sismos de Maca (1991), Sepina (1992) y Cabanaconde (1998), Región del Volcan Sabancaya (Arequipa). Bol. Soc. Geol. Peru 93, 63–72.

Barnes, I., Evans, W.C., White, L.D., 1978. Global distribution of CO2 and major zone of seismicity. In: US Geological Survey Open-File Report, 78–39.

Benavente, C., Delgado, G., García, B., Aguirre, E., Audin, L., 2017. Neotectónica, evolución del relieve y peligro sísmico en la Región Arequipa. In: INGEMMET. Boletín, Serie C, N°64. Geodinamica e Ingeniería Geológica, pp. 1–370.

Boixart, G., Cruz, L.F., Miranda Cruz, R., Euillades, P.A., Euillades, L.D., Battaglia, M., 2020. Source model for Sabancaya volcano constrained by DInSAR and GNSS surface deformation observation. Remote Sens. 12 (11), 1852. https://doi.org/10.3390/rs12111852.

Boschetti, T., Cifuentes, J., Iacumin, P., Selmo, E., 2019. Local Meteoric Water Line of Northern Chile (18° S–30° S): an Application of Error-in-Variables Regression to the Oxygen and Hydrogen Stable Isotope Ratio of Precipitation. Water 11(4), 791, 1–16. https://doi.org/10.3390/w11040791.

Can, I., 2002. A new improved Na/K geothermometer by artificial neural networks. Geothermics 31, 751–760.

Chiodi, A., Tassi, F., Báez, W., Maffucci, R., Invernizzi, C., Giordano, G., Corrado, S., Bicocchi, G., Vaselli, O., Viramonte, J.G., Pierantoni, P.P., 2015. New geochemical and isotopic insights to evaluate the geothermal resource of the hydrotermal system of Rosario de la Frontera (Salta, northern Argentina). J. Volcanol. Geotherm. Res. 295, 16–25. https://doi.org/10.1016/j.jvolgeores.2015.03.001.

Ciesielczuk, J., Żaba, J., Bzowska, G., Gaidzik, K., Głogowska, M., 2013. Surface mineralization at the geyser near Pinchollo, southern Peru. J. S. Am. Earth Sci. 53, 186–193. https://doi.org/10.1016/j.jsames.2012.06.016.

Ciesielczuk, J., Gaidzik, K., Paulo, A., Tyc, A., Postawa, A., Żaba, J., Masias, P., 2019. Thermal springs and active fault network of the central Colca River Basin, Western Cordillera, Peru. In: 8th International Symposium on Andean Geodynamics (ISAG), 24–26.09.2019, Quito, Ecuador.

Clark, I., Fritz, P., 1997. Environmental Isotopes in Hydrogeology. Lewis Publisher, New York, pp. 1–328.

Cortecci, G., Boschetti, T., Mussi, M., Herrera, C., Mucchino, C., Barbieri, M., 2005. New chemical and original isotopic data on waters from El Tatio geothermal field, northern Chile. Geochem. J. 39 (6), 547–571. https://doi.org/10.2343/geochemj.39.547.

Craig, H., 1961. Isotopic variations in meteoric waters. Science 133, 1702–1703. https://doi.org/10.1126/science.133.3465.1702.

Cruz, V., 2018. Chemical and isotopic composition of hot spring waters in the Tacna region, Southern Peru. In: INGEMMET Technical Report VCruz-001-2018.

Delgado, G., Benavente, C., Albinez, L., Aguirre, E., Taipe, E., 2016. Evaluación geológica post-sismo del 14 de agosto del 2016: reactivación de la falla Yanque. In: INGEMMET, Arequipa, pp. 1–83.

Farr, T.G., Kobrick, M., 2000. Shuttle Radar Topography Mission produces a wealth of data. Amer. Geophys. Union Eos 81, 583–585.

Field, C.W., Fifarek, R.H., 1985. Light stable-isotope systematics in the epithermal environment. Geology and geochemistry of epithermal systems. In: Berger, B.R., Bethke, P.M. (Eds.), Reviews in Economic Geology, 2, pp. 99–128.

Gaidzik, K., Więsek, M., 2021. Seismo-lineaments and potentially seismogenic faults in the overriding plate of the Nazca-South American subduction zone (S Peru). J. S. Am. Earth Sci. 109 doi:10910.1016/j.jsames.2021.103303.

Gaidzik, K., Żaba, J., Ciesielczuk, J., 2020. Tectonic control on slow-moving Andean landslides in the Colca Valley, Peru. J. Mt. Sci. 17 (8), 1807–1825. https://doi.org/10.1007/s11629-020-6099-y.

Gałaś, A., 2014. Petrology and new data on the geochemistry of the Andahua volcanic group (Central Andes, southern Peru). J. S. Am. Earth Sci. 56, 301–315. https://doi.org/10.1016/j.jsames.2014.09.012.

Gałaś, A., Paulo, A., Gaidzik, K., Zavala, B., Kalicki, T., Churata, D., Gałaś, S., Mariño, J., 2018. Geosites and geotouristic attractions proposed for the Project Geopark Colca and Volcanoes of Andagua, Peru. Geoheritage 10 (4), 707–729. https://doi.org/10.1007/s12371-018-0307-y.

Giggenbach, W.F., 1988. Geothermal solute equilibria. Derivation of Na-K-Mg-Ca geoindicators. Geochim. Cosmochim. Acta 52, 2749–2765. https://doi.org/10.1016/0016-7037(88)90143-3.

Giggenbach, W.F., 1991. Chemical techniques in geothermal exploration. In: D'Amore, F. (Ed.), Application of Geochemistry in Geothermal Reservoir Development. UNITAR, Rome, Italy, pp. 119–144.

Giggenbach, W.F., 1992. Isotopic shifts in waters from geothermal and volcanic systems along convergent plate boundaries and their origin. Earth Planet. Sc. Lett. 113, 495–510. https://doi.org/10.1016/0012-821X(92)90127-H.

González-Guzmán, R., Inguaggiato, C., Peiffer, L., Weber, B., Kretzschmar, T., 2019. Fault-controlled geothermal fluids of the northern Trans-Mexican Volcanic Belt: a geochemical and isotopic study of the Los Geysers field (Valley of Queretaro, Mexico). J. Volcanol. Geotherm. Res. 388, 106681 https://doi.org/10.1016/j.jvolgeores.2019.106681.

Huamaní, A., 2000. Aguas termales y minerales en el norte del Perú. In: INGEMMET Boletín D, 22, pp. 1–75.

Huamaní, A., 2001. Aguas termales y minerales en el suroriente del Perú (Dptos. Apurímac, Cusco, Madre de Dios y Puno). INGEMMET Boletín D 24, 1–172.

Huamaní, A., Valenzuela, G., 2003. Aguas termales y minerales en el oriente central del Perú (Dptos. Apurímac, Cusco, Madre de Dios y Puno). In: INGEMMET Boletín D, 25, pp. 1–86. http://desktop.arcgis.com/en/https://www.coreldraw.com/en/.

Jay, J.A., Delgado, F.J., Torres, J.L., Pritchard, M.E., Macedo, O., Aguilar, V., 2015. Deformation and seismicity near Sabancaya volcano, southern Peru, from 2002 to 2015. Geophys. Res. Lett. 42 (8), 2780–2788. https://doi.org/10.1002/2015GL063589.

Kukulak, J., Paulo, A., Kalicki, T., 2016. Lithology of lacustrine deposits in the Colca Valley. J. S. Am. Earth Sci. 69, 152–170. https://doi.org/10.1016/j.jsames.2016.03.008.

MacQueen, P., Delgado, F., Reath, K., Pritchard, M.E., Bagnardi, M., Milillo, P., Lundgren, P., Macedo, O., Aguilar, V., Ortega, M., Anccasi, R., Zerpa, I.A.L., Miranda, R., 2020. Volcano-tectonic interactions at Sabancaya Volcano, Peru: eruptions, magmatic inflation, moderate earthquakes, and fault Creep. J. Geophys. Res. Solid Earth 125 (5) e2019JB019281.

Mamani, M., Wörner, G., Sempere, T., 2010. Geochemical variations in igneous rocks of the Central Andean orocline (13°S to 18°S): tracing crustal thickening and magma generation through time and space. Geol. Soc. Am. Bull. 22 (1/2), 162–182. https://doi.org/10.1130/B26538.1.

Minissale, A., 2004. Origin, transport and discharge of CO_2 in Central Italy. Earth Sci. Rev. 66, 89–141. https://doi.org/10.1016/j.earscirev.2003.09.001.

Palacios, O., 1995. Geología histórica y evolución tectónica. Estratigrafía [in:] Geología del Perú. In: INGEMMET, Bol, 55, pp. 9–31.

Paulo, A., 2009. Idea general de estructura geológica de la Cordillera Occidental en el sur de Perú. In: Novoa, Z. (Ed.), Geología 2008 Expedicion Científica Polaca – Cañón del Colca: 37–54. Soc. Geogr. de Lima.

Pérez-Flores, P., Cembrano, J., Sánchez-Alfaro, P., Veloso, E., Arancibia, G., Roquer, T., 2016. Tectonics, magmatism and paleo-fluid distribution in a strike-slip setting: Insights from the northern termination of the Liquiñe-Ofqui fault System, Chile. Tectonophysics 680, 192–210. https://doi.org/10.1016/j.tecto.2016.05.016.

Piper, A.M., 1944. A graphic procedure in the geochemical interpretation of water analyses. Am. Geophys. Union Trans. 25, 914–923. https://doi.org/10.1029/TR025i006p00914.

Reath, K., Pritchard, M., Biggs, J., Andrews, B., Ebmeier, S.K., Bagnardi, M., Girona, T., Lundgren, P., Lopez, T., Poland, M., 2020. Using conceptual models to relate multiparameter satellite data to subsurface volcanic processes in Latin America. Geochem. Geophys. 21 (1), e2019GC008494 https://doi.org/10.1029/2019GC008494.

Rivera, M., Mariño, J., Samaniego, P., Delgado, R., Manrique, N., 2015. Geología y evaluación de peligros del complejo volcánico Ampato-Sabancaya (Arequipa). In: INGEMMET Boletín Serie C Geodinámica e Ingeniería Geológica, 61, p. 122.

Romano, P., Liotta, M., 2020. Using and abusing Giggenbach ternary Na-K-Mg diagram. Chem. Geol. 541, 119577 https://doi.org/10.1016/j.chemgeo.2020.119577.

Roquer, T., Arancibia, G., Rowland, J., Iturrieta, P., Morata, D., Cembrano, J., 2017. Fault-controlled development of shallow hydrothermal systems: structural and mineralogical insights from the Southern Andes. Geothermics 66, 156–173. https://doi.org/10.1016/j.geothermics.2016.12.003.

Różański, K., Araguas-Araguas, L., Confiantini, R., 1993. Isotopic patterns in modern global precipitation. In: Climate Change in Continental Isotopic Records Geophysical Monograph, 78, pp. 1–36.

Sacchi, E., Zuppi, G.M., Pizzino, L., Quattrocchi, F., Lombardi, S., 2008. Fluid geochemistry as indicator of tectonically-related, deep water circulations in the Sardinian Rift-Campidano Graben (Italy): new insights from environmental isotopes. Aquat. Geochem. 14 (4), 301–319. https://doi.org/10.1007/s10498-008-9038-z.

Samaniego, P., Rivera, M., Mariño, J., Guillou, H., Liorzou, C., Zerathe, S., Delgado, R., Valderrama, P., Scao, V., 2016. The eruptive chronology of the Ampato–Sabancaya volcanic complex (Southern Peru). J. Volcanol. Geotherm. Res. 323, 110–128. https://doi.org/10.1016/j.jvolgeores.2016.04.038.

Santoyo, E., Díaz-González, L., 2010. A new improved proposal of the Na/K geothermometer to estimate deep equilibrium temperatures and their uncertainties in geothermal system. In: Proceedings World Geothermal Congress, Bali, Indonesia, 25–29 April 2010, 1–9.

Sebrier, M., Mercier, J.L., Megard, F., Laubacher, G., Carey-Gailhardis, E., 1985. Quaternary normal and reverse faulting and the state of stress in the Central Andes of South Peru. Tectonics 4 (7), 739–780. https://doi.org/10.1029/TC004i007p00739.

Steinmüller, K., 2001. Modern hot springs in the southern volcanic Cordillera of Peru and their relationship to Neogene epithermal precious-metal deposits. J. S. Am. Earth Sci. 14, 377–385. https://doi.org/10.1016/S0895-9811(01)00033-5.

Steinmüller, K., Huamani, A., 1999. Aguas termales y minerales en el centro del Perú. In: INGEMMET Boletín D 21, pp. 1–76.

Steinmüller, K., Nuñez, S., 1998. Hidrotermalismo en el sur del Perú, sector Cailloma-Puqio. In: INGEMMET Boletín D, 19, pp. 1–106.

Steinmüller, K., Zavala, B., 1997. Hidrotermalismo en el sur del Perú. In: INGEMMET Boletín D, 18, pp. 1–79.

Tassi, F., Vaselli, O., Moratti, G., Piccardi, L., Minissale, A., Poreda, R., Tedesco, D., 2006. Fluid geochemistry versus tectonic setting: the case study of Morocco. Geol. Soc. Lond., Spec. Publ. 262 (1), 131–145. https://doi.org/10.1144/GSL.SP.2006.262.01.08.

Townend, J., Sutherland, R., Toy, V.G., Doan, M.-L., Célérier, B., Massiot, C., Coussens, J., Jeppson, T., Janku-Capova, L., Remaud, L., Upton, P., Schmitt, D.R., Pezard, P., Williams, J., Allen, M.J., Baratin, L.-M., Barth, N., Becroft, L., Boese, C. M., Boulton, C., Broderick, N., Carpenter, B., Chamberlain, C.J., Cooper, A., Coutts, A., Cox, S.C., Craw, L., Eccles, J.D., Faulkner, D., Grieve, J., Grochowski, J., Gulley, A., Hartog, A., Henry, G., Howarth, J., Jacobs, K., Kato, N., Keys, S., Kirilova, M., Kometani, Y., Langridge, R., Lin, W., Little, T., Lukacs, A., Mallyon, D., Mariani, E., Mathewson, L., Melosh, B., Menzies, C., Moore, J., Morales, L., Mori, H., Niemeijer, A., Nishikawa, O., Nitsch, O., Paris, J., Prior, D.J., Sauer, K., Savage, M.K., Schleicher, A., Shigematsu, N., Taylor-Offord, S., Teagle, D., Tobin, H., Valdez, R., Weaver, K., Wiersberg, T., Zimmer, M., 2017. Petrophysical, geochemical, and hydrological evidence for extensive fracture-mediated fluid and heat Transport in the Alpine fault's hanging-wall damage zone. Geochem. Geophys. Geosyst. 18, 4709–4732. https://doi.org/10.1002/2017GC007202.

Tyc, A., Gaidzik, K., Paulo, A., Żaba, J., Ciesielczuk, J., 2021. Structural setting and genesis of collapse features in travertines of Huambo (Peruvian Andes). In: XII Zjazd Geomorfologów Polskich. Abstract Book, Gdańsk, Poland, pp. 204–205.

Valdivielso, S., Vázquez-Suñé, E., Custodio, E., 2021. Isotopía ambiental de las precipitaciones y de las aguas superficiales y subterráneas en los Andes Centrales: Revisión. Bol. Geol. Min. 132 (1–2), 147–156.

Vargas, V., 2010. Las fuentes termales en el Peru, estado y uso actual. In: XV Congreso Peruano de Geología. Resúmenes Extendidos. Soc. Geol. del Perú. Pub. Esp. 9, 1175–1178. Cusco.

Vargas, V., Cruz, V., 2010. Geothermal Map of Perú. Proceedings World Geothermal Congress, Bali, Indonesia, 25–29 April 2010, pp. 1–7.

Verma, S.P., Santoyo, E., 1997. New improved equations for Na/K, Na/Li and SiO2 geothermometers by outlier detection and rejection. J. Volcanol. Geotherm. Res. 79, 9–23.

Waring, G.A., 1965. Thermal springs in the United States and other countries of the world – a summary. In: Geological Survey Professional Paper 492. United States Government Printing Office, Washington.

Wells, D.L., Coppersmith, K.J., 1994. New empirical relationships among magnitude, rupture length, rupture width, rupture area, and surface displacement. Bull. Seismol. Soc. Am. 84 (4), 974–1002.

Wohletz, K., Heiken, G., 1992. Volcanology and Geothermal Energy. Univ. of California Press, Berkeley and Los Angeles, pp. 1–432.

Wrage, J., Tardani, D., Reich, M., Daniele, L., Arancibia, G., Cembrano, J., Sánchez-Alfaro, P., Morata, D., Pérez-Moreno, R., 2017. Geochemistry of thermal waters in the Southern Volcanic Zone, Chile – Implications for structural controls on geothermal fluid composition. Chem. Geol. 466, 545–561. https://doi.org/10.1016/J.CHEMGEO.2017.07.004.

Yardley, B.C., Bodnar, R.J., 2014. Fluids in the Continental Crust. Geochem. Perspect. 3 (1), 1–127.

Żaba, J., Małolepszy, Z., Gaidzik, K., Ciesielczuk, J., Paulo, A., 2012. Fault network in Rio Colca valley between Maca and Pinchollo, Central Andes, southern Peru. Ann. Soc. Geol. Pol. 82, 279–290.

Żaba, J., Gaidzik, K., Ciesielczuk, J., Paulo, A., Głogowska, M., 2013. Tectonic relationships between travertine domes and underlain Mesozoic formations in Huambo vicinity, southern Peru. In: Proceedings of the 11th Meeting of the Central European Tectonic Studies Group (CETeG), 24–27.04.2013, Vargesztes, Villa Park, Hungary.

Zarrouk, S.J., McLean, K., 2019. Geothermal Well Test Analysis: Fundamentals, Applications and Advanced Techniques. Elsevier, Academic Press.

Zavala, B., Vilchez, M., Rosado, M., Pari, W., Peña, F., 2014. Estudio geoambiental en la Cuenca del Rio Colca. In: INGEMMET Bol. Serie C, 57, pp. 1–222.